J. Fluid Mech. (1998), *vol.* 373, *pp.* 81–110. Printed in the United Kingdom

© 1998 Cambridge University Press

Front dynamics and fingering of a driven contact line

By IGOR VERETENNIKOV, ALEXANDRA INDEIKINA AND HSUEH-CHIA CHANG

Department of Chemical Engineering, University of Notre Dame, Notre Dame, IN 46556, USA

(Received 11 April 1997 and in revised form 27 May 1998)

Using photographic imaging and dye tracking experiments, we scrutinize the dynamics of a contact line when a finite volume of partially wetting fluid is driven by gravity to spread over a slightly inclined dry plane. Unlike spreading mechanisms driven by molecular forces, gravity-driven spreading over a dry plane is shown to possess a characteristic interfacial 'nose' that overhangs the contact line when the film thickness is in excess of the capillary length. A unique recirculating vortex exists within the nose front which spreads at speeds corresponding to capillary numbers in excess of 10^{-2}. Our experiments show that fingering from a gravity-driven straight front occurs when the above nose configuration cannot be sustained across the entire front as the film thins and the apparent contact angle θ reaches $\pi/2$. The fingers retain the nose configuration while the remaining segments of the front evolve into a wedge configuration and stop abruptly due to their large resistance to fluid flow. This fingering mechanism is insensitive to fluid wettability, noise or surface heterogeneity. Via matched asymptotics, we obtain accurate estimates of fingering position and speed at $\theta = \pi/2$ that are in good agreement with measured values. This new mechanism is distinct from other instability and sensitivity fingering mechanisms and can be in play whenever θ of the straight front approaches $\pi/2$ from above as the film thins.

1. Introduction

1.1. *Contact line dynamics and interfacial geometry*

The spreading of a liquid over a dry solid is an interesting and important phenomenon that remains difficult to model and understand. Without special consideration, computed stress and pressure can become infinite at the contact line (Ludviksson & Lightfoot 1968; Huh & Scriven 1971) due to a breakdown of the usual fluid mechanical assumptions in this region (Hansen & Toong 1971; Dussan V. & Davis 1974; Dussan V. 1976). Over the years, several models have been proposed to remove this unrealistic singularity.

One proposed physical model is to assume the existence of a microscopic precursor film in front of the moving macroscopic liquid wedge of a wetting fluid. Long-range intermolecular forces are shown to create a negative 'disjoining pressure' (relative to the ambient air pressure) which, together with the capillary pressure, is responsible for sucking liquid from the bulk into the front-running precursor film (de Gennes 1985). The precursor film (about 10 nm thick and a few mm long) has been detected by Bascom, Cottington & Singleterry (1964), for example, by ellipsometry during late-stage spreading of completely wetting non-polar liquids on steel.

For such spontaneous spreading processes driven by molecular forces, the capillary number $Ca = \mu\hat{u}/\sigma$, where $\hat{u}$ is the spreading speed, is typically less than 10^{-3}. The apparent contact angle θ, measured from the liquid side is very close to the static value θ_e and the interface near the contact line is wedge shaped. For sufficiently fast spreading driven by gravity or other external forces, however, the precursor film model does not seem to apply (Neogi & Abib 1985). This is especially true for partially wetting fluids.

Under forced spreading, the dynamic contact angle can be very different from the static one and Ca is typically several orders of magnitude higher than in the case of spontaneous spreading. One of the most complete experimental studies of how spreading viscous fluids displace air has been carried out by Hoffman (1975) in a capillary. In his experiments, five orders of magnitude of the capillary number are covered ($4 \times 10^{-4} \leqslant Ca \leqslant 36$) for both completely and partially wetting fluids, while inertial effects are maintained at a negligible level. Within the accuracy of his microphotographic technique, he does not detect any deviation of the meniscus from a spherical shape. Apparent contact angles, measured by extrapolating the spherical meniscus, start from zero at zero Ca for completely wetting fluids and from their advancing values for partially wetting fluids. They exceed $\pi/2$ beyond $Ca \approx 4.9 \times 10^{-2}$ for all completely wetting fluids and beyond $Ca \sim 2 \times 10^{-2}$ for two partially wetting fluids with $\theta_e \sim 70°$. All contact angles reach the maximum value of $\theta = \pi$ beyond $Ca \gtrsim 4$.

Even though Hoffman's study is carried out with a capillary, the conclusion that, regardless of the liquid wetting properties, motion with $\theta > \pi/2$ is very prevalent for forced spreading over a large range of practical $Ca \gtrsim O(10^{-2})$ remains valid for other geometries, including the important case of an advancing straight front. For this planar geometry, the interface should resemble a nose that overhangs the straight contact line for $\theta > \pi/2$ and a wedge for $\theta < \pi/2$. While the precursor film may exist in front of a wedge, it is unlikely to appear before a nose because it would require unreasonably large interfacial curvatures, as pointed out by Neogi & Abib (1985).

1.2. *Recirculation in a nose and implications*

The flow fields within a nose and a wedge should also be fundamentally different at a macroscopic scale away from the contact line. If θ is very small, the thin wedge should sustain a lubrication-type flow field which is unidirectional and parabolic. Within the nose, however, a recirculating vortex is expected. Yarnold (1938) has observed recirculation within mercury boluses through a capillary and non-wetting mercury drops down an inclined plane with $\theta > \pi/2$. Dussan V. & Davis (1974) propose that an advancing fluid undergoes a 'rolling' type motion, i.e. that a material point arrives in finite time at the triple line from the fluid–fluid interface and then remains adhered to the solid, regardless of the interfacial shape. They report several qualitative dye tracking experiments for different fluid/fluid/solid systems to confirm such kinematics of material points near the moving triple contact line. From their analysis, it follows that nose and wedge motion are kinematically identical and that macroscopic no-slip boundary conditions for both fluids in the contact line region lead to non-integrable stress singularities. However, photographs shown in their article, for both liquid/liquid/solid systems and the only liquid/gas/solid system with a honey drop moving down an inclined Plexiglas plane, clearly show nose-shaped fronts that overhang the contact line.

An even more complex fluid motion has been detected by Allen & Benson (1975). A small drop of water (less than 1 cm in diameter) is placed on a horizontal glass

plane, which is then inclined until the drop runs down the plane. It is observed that, in this case of highly-wetting liquid, the 'fluid particles on the gas/liquid interface remained there, forming a kind of surface skin'. This skin does not roll although a complicated three-dimensional vortex motion within the drop has been detected. It is also reported that 'observation of dust particles and dye on the surface of the mercury drop which is moving down the plane showed a purely circular or rolling motion with the plane of motion parallel to the direction of flow and normal to the inclined plane'. Allen & Benson (1975) propose that 'whether the surface skin rolls or slides may well depend on the advancing contact angle being greater or less than $\pi/2$'.

While the 'kinematics' of interfacial material elements may be identical, the difference in macroscopic vortex motion within a nose and macroscopic unidirectional flow within a wedge reflects the different driving and resistance forces present in contact line motion. A macroscopic vortex motion within a nose means that a fluid element immediately above the contact line is falling towards the solid in the upstream direction relative to the front motion. This implies that molecular forces, which only act to move the liquid in the downstream direction, contribute negligibly to the motion of a nose. This is consistent with the speculation of Neogi & Abib (1985) that forced spreading dynamics with $\theta > \pi/2$ is independent of fluid wettability and static contact angle θ_e, both of which are governed by molecular forces. In a moving liquid wedge, macroscopic unidirectional flow is necessary to sustain the shape of the front. The motion of fluid particles 'from air–liquid to solid–liquid interface' should occur in a microscopic region near the real contact line. Hence, molecular forces are of paramount importance in the macroscopic motion of a wedge even if it is also driven by some external force. Consequently, a wedge front would be sensitive to surface heterogeneity and roughness. The opposite would be true of a nose front. More importantly, since a narrow wedge must exist down to microscopic scales in a wedge front, one expects the resistance to liquid flow to be much larger in a wedge front compared to a nose front. Hence, the above differences in the macroscopic flow field near the front have profound implications on the front dynamics and, as we shall demonstrate, the front's propensity to finger.

1.3. *Fingering instability of gravity-driven contact line*

Fingering from the straight contact line of a front driven by an external force has been a recent topic of interest (Huppert 1982; Troian *et al.* 1989; Spaid & Homsy 1996; Bertozzi & Brenner 1997). There is considerable debate over the fingering mechanism. In particular, whether an instability exists and how a specific finger separation is selected remain controversial. Nevertheless, it is generally agreed that only fronts with a permanent bump above the contact line are unstable. All earlier fingering theories have, however, examined only wedge fronts. The single-valued interfacial height of the wedge near the contact line has often been assumed to be slowly varying such that a long-wave lubrication expansion can be carried out to resolve the nearly unidirectional flow within the wedge. However, discussions in the previous subsection suggest that this long-wave approximation is only valid for macroscopic wedges of highly wetting liquids for which molecular forces are important to the contact-line dynamics. In fact, sensitivity to surface heterogeneity, which is necessary to trigger the transient growth mechanism proposed by Bertozzi & Brenner (1997), requires a single-valued wedge. Studies (Goodwin & Homsy 1991) have been carried out without a long-wave expansion but a macroscopic wedge is

still assumed. However, typical capillary numbers in fingering experiments are of the order of 10^{-2}–10^{-1} (de Bruyn 1992; de Bruyn & Jerret 1992). At this high Ca range, most contact angle measurements would suggest that a nose front is present. It is then quite conceivable that a thick (larger than the capillary length) gravity-driven front, containing even a highly wetting liquid with a small static contact angle, will have a multi-valued nose (with $\theta > \pi/2$) on a dry plane. Hence, fingering for the most common thick fronts at small inclination angles is still not understood.

1.4. *Present results*

In §§2 and 3 we describe our experiments and report glycerine and Castor oil fingering data on dry and pre-wetted planes for relatively thick ($h \sim 3$–5 mm) gravity-driven fronts at low inclination angles ($4^\circ \leqslant \alpha \leqslant 14^\circ$). The front speed at the onset of fingering yields a relative large capillary number, $2.9 \times 10^{-2} < Ca < 8.4 \times 10^{-2}$. Prior to fingering and immediately after the commencement of motion, the capillary number is even higher at a few times 10^{-1}. For such conditions, we detect a distinct multi-valued nose above the moving contact line on a dry plane for both the glycerine and Castor oil used. On a pre-wetted plane, only a wedge shape is detected for the Castor oil front. We find that, regardless of the wetness of a plane, a bump does not appear on the front at any time prior to fingering at $\alpha \leqslant 14^\circ$. We observe that fingering from a nose front on a dry plane occurs at a specific downstream position and at a specific front speed, both of which are insensitive to surface heterogeneity. The existence of a critical speed, below which the motion of a straight nose front is impossible, is established experimentally with fronts driven at constant speeds. We also perform a few qualitative dye tracking experiments to visualize the difference in the flow field within wedge and nose fronts and within developed fingers. It is established that, on a dry plane, a recirculating vortex motion exists within the nose front in the laboratory frame of reference and that the developed fingers retain the nose configuration and continue to move in the same manner as a straight front. Macroscopic flow in a wedge is, however, unidirectional.

In §4, we summarize our experimental observations and propose a physical mechanism for the motion of a nose front and fingering on a dry plane. We suggest that fingering occurs at a specific front speed when the apparent contact angle θ is equal to $\pi/2$ due to local changes in the mechanism of spreading along the front since at this point the entire front cannot retain a nose configuration. Because of the difference in their flow resistance, the segments along the contact line with θ slightly less than $\pi/2$ decelerate rapidly relative to segments with θ slightly larger than $\pi/2$. Transverse curvature suppresses short-wavelength deviations but this mechanism does not select any specific wavelength. Instead, almost identical fingers shoot out locally without significant interaction. Our new fingering mechanism for bumpless nose fronts yields a fingering position that is insensitive to either initial nose or surface heterogeneity. We support the proposed critical contact angle, $\theta_c = \pi/2$, with a theoretical analysis. Using matched asymptotics, we obtain the evolution of the contact angle, front position and speed in time. The critical condition $\theta_c = \pi/2$ then yields predictions of the front position and speed at fingering that are in good agreement with our measurements over a wide range of conditions.

In §5, we discuss implications of this new fingering mechanism and possible extensions to further scrutinize the fingering dynamics. We also offer some discussion of fingering on prewetted planes.

2. Experimental setup and imaging techniques

2.1. *Experimental apparatus*

Two experimental apparatuses are constructed for our fingering experiments. The first one is conceptually similar to earlier ones for gravity-driven spreading (Goodwin 1991). A Plexiglas plane 91 cm long in the downstream x-direction, 46 cm wide and about 1 cm thick is affixed to an aluminium frame and is allowed to tilt at an angle α between 0° and 14° from the horizontal. The plane is tilted in the opposite direction (negative angle) initially up to about -5° from the horizontal. The liquid (volume $V \sim 100$ to 250 ml) is poured into a small three-sided compartment at the back end. After a waiting period of about a few minutes, the plate is slightly rotated to equilibrate the liquid and create an almost straight front. The inclination angle is still negative and is about -2° from the horizontal. Using the same protocol (Goodwin 1991) for every run, the plane is slowly rotated to the desired angle to initiate the experiment. For the liquid volume used, the front thickness up to fingering is always in excess of the effective capillary length $H = (\sigma/\rho g \cos\alpha)^{1/2}$ of about 2.3 mm and 2.1 mm respectively for the glycerine and Castor oil used.

The second apparatus is designed for mechanically driven fronts which propagate at a constant velocity. A Plexiglas plane 85 cm long in the downstream x-direction, 46 cm wide and about 1 cm thick is mounted on a special plane made from aluminium extrusions. Two parallel rods are mounted along the side of the aluminium plane. A narrow Plexiglas plate (40.64 cm wide and 5 cm high) is then mounted transversely across the plane and mounted with flanged recirculating ball linear bearings on the rods. The gap between the driving plate and the plane is sealed with nylon wear stripes on a small aluminium frame to reduce leakage from the moving plate to a negligible trickle. A 95 cm long precision ACME threaded rod (5 pitch per in.) is used to guide the linear motion of this driving plate. The rod itself is connected to a DC motor with a 5-to-1 gear box mounted at the far end of the plane. To ensure constant driving speed, a magnetic frequency pick-up is mounted on the thread rod to measure the rotating frequency of the rod and this input is fed back to a speed controller connected to the DC motor. In this manner, the rod rotation frequency can be varied from almost 0 up to 500 r.p.m., corresponding to a driving plate speed up to 4.2 cm s^{-1}, with a $\pm 1/2$ r.p.m. long time error. The stability of the rotation is unacceptable when the frequency is lower than 40 r.p.m., which corresponds to a speed of 0.34 cm s^{-1}, since our sensor provides only one pulse per rotation and the motor imparts unacceptable low momentum. Frequencies higher than 150 r.p.m., which correspond to speeds in excess of 1.27 cm s^{-1}, are never used because the curved front flattens to a straight one if the pushing speed is higher than 1 cm s^{-1}or the frequency of rotation is higher than 120 r.p.m. Two limit switches are used to limit the working region along the plane to about 70 cm long.

2.2. *Fluid and plane preparation*

Glycerine and Castor oil are used as the experimental liquids. Glycerine has a high static contact angle on Plexiglas ($\theta_e \sim 50^\circ - 70^\circ$) and is partially wetting while Castor oil with $\theta_e \sim 10^\circ$ is almost wetting. The glycerine viscosity can change significantly due to the absorption of water. Viscosity measurement is hence carried out before each run by using an EZ viscosity cup with an error less then 10%. Because viscosity variations of glycerine can be caused by a very small amount of water and because the surface tensions of both liquids are close, we assume that the surface tension of glycerine remains constant and does not depend on the water composition. The

surface tensions of glycerine and Castor oil are taken from the literature to be $\sigma \approx 63.4$ mN m^{-1}and 33.1 mN m^{-1}, respectively.

Prior to each run, the planes are cleaned with water and detergent and then allowed to dry in air. After drying, the plane is washed with almost pure ethyl alcohol, finally cleaned with commercial surface cleaner and again dried in air afterwards. This procedure is used to create a dry and chemically uniform surface. In cases when a pre-wetted plane is desired, half a litre of the liquid is first poured onto the plane and manually spread over the entire plane. This film is not generally uniform in thickness. A half litre of the liquid is then poured again onto the plane which is tilted to allow the liquid film to drain and thin. Depending on the time of drainage, uniform pre-wetted films of arbitrary thickness can be manufactured in this manner. For the thinnest films, drainage overnight is necessary. Unfortunately, we are not able to measure the film thickness created this way and drainage time is the only qualitative measure of the film thickness. However, the pre-wetted plane behaves in a manner that is different from a dry one during fingering. Since only highly wetting liquids can sustain a flat thin film without dewetting, planes can only be pre-wetted with Castor oil and not glycerine.

2.3. *Front imaging*

The profile and top view of the advancing contact line and fingers are photographed with a high-resolution Kodak MegaPlus 1.6 digital camera at a time interval of about 3 s. A special code was developed to record images onto the hard disk of a Power PC Macintosh 7100/66 computer. Image analysis is performed using public domain NIH Image program (developed at the US National Institute of Health and available on the Internet at http://rsb.info.nih.gov/nih-image/) and MATLAB by The MathWorks Inc. The apparatus with a mechanical drive does not permit a side view due to the presence of the guiding rods. Its top view is also partially obscured by the driving rod.

Dyes are used to enhance the imaging quality of the contact line and fingers. For Castor oil, Sudan IV is used to produce a liquid with a rich red colour. The plane itself is pre-wetted with pure transparent Castor oil if a pre-wetted plane is desired. Front distortion due to dye diffusion is negligible. For glycerine, a Fluorescein sodium salt has been mixed uniformly within the glycerine and induced to glow with a black light lamp. The Indulin B is also used for profile imaging of glycerine front and dye tracking experiments. We should mention that the coloured Castor oil is slightly heavier than pure Castor oil while the density of coloured glycerine almost does not change.

We find that estimating the film height with fluorescence intensity measurements from top imaging can be misleading. For example, when we place a black light lamp parallel to the moving front and record the image overhead, a bump is seen in the intensity profile near the moving contact line. Removal of the lamp also removes the intensity bump. Another problem with thickness estimation from the fluorescence intensity measurements is that the intensity is proportional to an integral of some function of the dye concentration in the liquid over the film thickness. To solve the inverse problem and obtain the film thickness, we should then make *a priori* assumptions about the surface shape since a single-valued wedge and a multi-valued nose of similar thickness can produce almost indistinguishable intensity profiles. We should mention that a multi-valued nose also introduces the strong additional effect of interfacial curvature which focuses or diffuses fluorescence light. A similar lens effect can also occur in a single-valued wedge with a high bump. In the case of a

wedge without a bump, the curvature is lower and this lens effect can be small. It is possible to take into account the curvature effect, but again *a priori* assumptions about the surface shape are needed. We hence choose to carry out our profile imaging from the side. To eliminate reflection of the fluorescence light from the Plexiglas plane and to remove all uncertainties regarding the interface shape near the contact line caused by the lens effect, we used Indulin B (dark blue) as a dye to enhance the quality of the side photographs of the spreading glycerine front.

2.4. *Dye tracking for flow field visualization*

For flow field visualization, a small drop of dye is mixed in glycerine or Castor oil and placed at the top of the transparent film and allowed to be convected by the interfacial flow, as in the dye tracking experiment of Dussan V. & Davis (1974). Positions of the dye drop are photographed with our digital camera. Hence, the contact line positions at the instant the front (or back) end of this drop reaches the contact line can be determined and marked on subsequent frames. Because of the limitations of the camera, the smallest time interval between two frames is about 1.5 s. Hence, these experiments are usually repeated a few times and several dye drops are used to detect all characteristic features of the flow within the nose and wedge fronts.

There should be a big difference between the flow within the multi-valued nose and the wedge. The front part of the nose moves like a deformable wheel. At the point of contact, the instantaneous velocity is equal to zero. At the next instant of time, a new contact line is created as the nose again touches the plane. Hence, the dye droplet should keep its shape when it lands on the plane. However, due to the finite thickness of the drop, some dye that is initially located just below the air–liquid interface will not touch the solid but will be convected in the direction of the flow just above the plane, i.e. upstream. Hence, if a vortex really exists inside the nose front, we should expect the dye to be stretched behind (upstream of) the point where the leading edge of the drop first touches the plane. The rear boundary of the drop, however, is expected to stay in place where it touches the plane. Similar to the motion of a wheel, the vortex also introduces an upward flow behind the moving nose front. This flow raises the dye from the upper parts of the landing drop almost to the air–liquid interface and then convects it downstream towards the nose region again. As the dye reaches the nose, it will again rotate, thus forming distinct loops of dye streak. The separation between these loops is determined by the time it takes the dye to undergo a complete circuit.

Consider, instead, the wedge motion. The dye drop from the air–liquid interface will also reach the plane but the signature of how it lands should be different. In the wedge, flow is expected to be unidirectional up to a microscopic region near the actual contact line. As has been shown by de Gennes (1985), a thin pre-wetted film on a plane is qualitatively similar to a very thick precursor film. A small region, about the order of thickness of the pre-wetted film, exists near the junction of the macroscopic wedge front with the film, and it corresponds to the contact line region in this case. Hence, because of the macroscopic unidirectional flow that extends into this small region, one should not find any dye behind the position where the leading edge of the drop first touches the plane. Also, one can expect the front part of the droplet to move forward with respect to the position of first contact between the dye drop and the plane. Eventually, the entire dye drop will be stretched in the lower layers of the liquid. Hence, if recirculation is absent in a wedge, slightly heavier coloured liquid could not be lifted to the top surface of the current and will never reach the front again. Loops of dye steak can hence only appear in a vortex flow field and not in a unidirectional one.

3. Experimental results

3.1. *Flow within nose fronts and fingers on a dry plane*

Typical profiles of a spreading, pre-fingering glycerine front on a dry plane are shown in figure 1(*a*). A bump is clearly absent and the protruding nose beyond the advancing contact line is evident. Due to reflection off the plane, a mirror image of the profile also appears below the front. Nevertheless, it is still evident that the nose intersects the solid plane at an apparent contact angle $\pi > \theta > \pi/2$ prior to fingering. This contact angle θ decreases towards $\theta_c = \pi/2$ although this is not very apparent in figure 1(*a*). A wedge shape with $\theta < \pi/2$ is never observed near a straight front in the case of a dry solid surface for both Castor oil and glycerine.

A small drop of dye ($\sim$ 0.05 cm^3) is placed at the top of the interface behind the advancing glycerine front ($\theta_e \sim 60°$) in figure 2. The interfacial flow field clearly flattens and advects it towards the contact line along the top of the interface without much distortion (figure 2*b*). The two-dimensional circular drop is eventually rolled below the liquid such that it ends up on the solid plane after being rotated around the nose (frame *c* in figure 2). Finally, the complete drop lands on the plane and the dye is left on the solid by the advancing front (figure 2*f*). The vortex motion observed earlier by Yarnold (1938), Dussan V. & Davis (1974) and Allen & Benson (1975) within the nose is hence established. A schematic representation of this recirculation of the liquid within the nose is shown in figure 1(*b*). A Sobel filter has been applied to some frames in figure 2 for better resolution of the boundary of the dye spot and the contact line. The dashed lines in figure 2(*c–f*) show the position of the contact line from figure 2(*b*) at the moment when the dye drop touches the plane. The dash-dotted lines in figures 2(*e*) and 2(*f*) record the position of the contact line from figure 2(*d*), when a complete drop lies on the plane as the back end of the drop reaches the contact line. As is evident from the relative position of the dash-dotted line and the sharp boundary of the dye spot in figure 2(*e*), there is an appreciable interval when the dye remains at the same position, while the front has clearly moved forward. Back and forth motion of the dye droplet during the 1.5 s time interval between frames (*d*) and (*e*) in figure 2 is unlikely since such motion should produce a diffused drop boundary, like in figure 2(*f*). It is also evident from figures 2(*d*) and 2(*e*), that there is no stretching of the drop under the moving nose front. The stretching of the dye spot occurs only behind the advancing nose front, as it evident from figure 2(*f*). The stretching occurs because the flow field within the flat film region behind the front is again unidirectional with high wall shear while there is almost no shear within the nose. The relative positions of the dashed line and diffused boundary of the dye spot in figure 2(*c–f*) indicate that there is a backward upstream flow near the plane under the moving nose front – the flow field is not unidirectional, but recirculating, as discussed in the previous section.

Dye tracking of the almost wetting Castor oil ($\theta_e \sim 10°$) gravity current on a dry Plexiglas plane is shown in figures 3 and 4. In figure 3(*a*) both drops are lying on the top surface of the current. In the next frame (*b*), the 'upper' drop lies almost completely on the plane while the 'lower' one only begins its rotation around the nose. In figure 3(*c–e*) the upper drop is left behind the advancing finger that has developed. One can also clearly see how the lower drop rotates around the nose, forming distinct dye loops. The difference in dye stretching between glycerine (figure 2) and Castor oil (figure 3) is due to the dye properties. The coloured Castor oil is slightly heavier than the pure one, while the coloured glycerine has almost the same density as the pure liquid. Hence, when a drop of coloured Castor oil is placed on the free surface

(*a*)

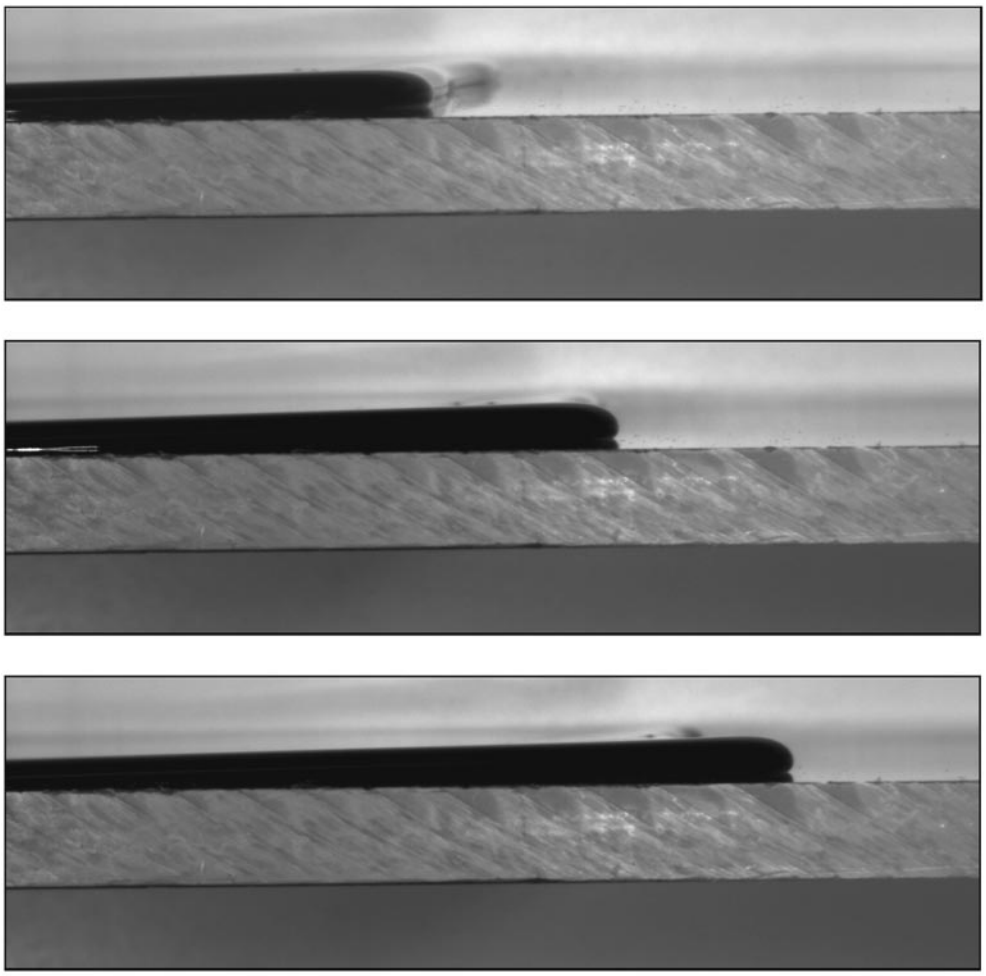

(*b*)

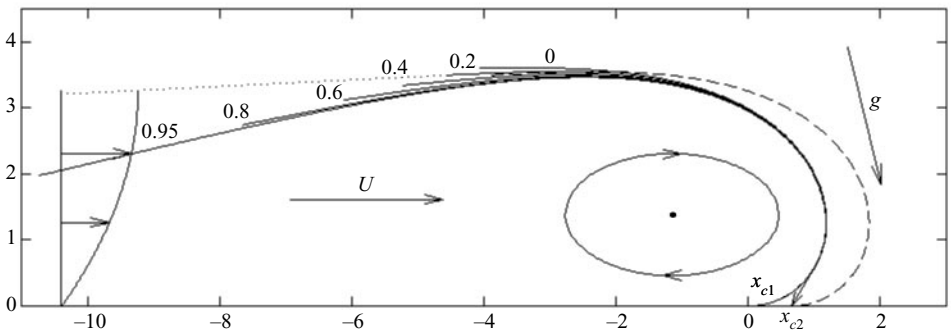

FIGURE 1. Typical profiles of a gravity-driven front. (*a*) Glycerine is the experimental liquid, $\alpha = 14°$, $\nu = 5.25$ cm^2 s^{-1} and $V = 175$ ml. Images are taken every 1.5 s. The thickness of the Plexiglas plane is 0.8 cm. (*b*) Schematic representation of the vortex motion of the liquid within the multi-valued nose. Huppert's tail solution (· · ·) and the front position at the next instant of time (- -) are also sketched. The nose shape is represented by the solution of the Young–Laplace equation at $\alpha = 14°$. The corresponding values of (φ_i/α) are indicated where φ_i is the tangent angle at the inflection point where $\varphi_s = 0$. The nose shape is insensitive to φ_i. The evolving and thinning front on a plane corresponds to a shift of the base line upwards as θ decreases.

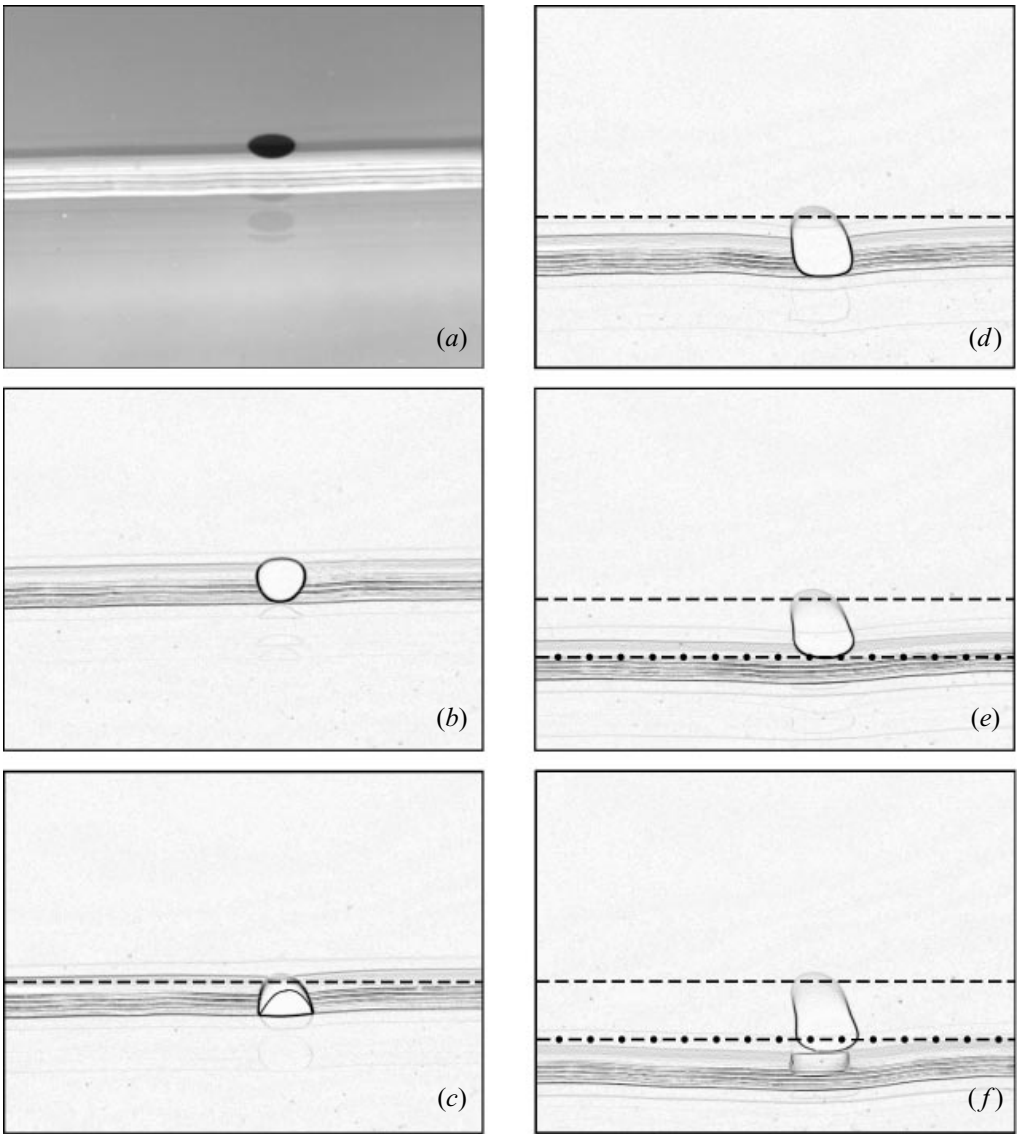

FIGURE 2. Motion of a small drop of dye from its initial position near the top of the interface behind the advancing glycerine front under conditions $(\alpha, \nu, V) = (4^\circ,\ 6.67\ \mathrm{cm}^2\ \mathrm{s}^{-1},\ 200\ \mathrm{ml})$. The pancake-shaped dye is advected around the nose and contact line and left on the solid plane. Stretching only occurs when the dye reaches the solid. The position of the contact line from frames (*b*) (- - , when the drop touches the plane) and (*d*) (- · -, when the entire drop lies on the plane) are shown. Images are taken every 1.5 s.

of the current, part of the drop goes down into the slower moving layers of liquid and significant stretching occurs even before the dye reaches the front.

Similar dye tracking of the Castor oil front and fingers on a dry Plexiglas plane for a larger time interval is shown in figure 4. Figure 4(*a*) corresponds to the moment when the upper drop of dye touches the plane while two other drops are still on the surface. In figure 4(*b*), all dye spots are near the bottom and they are left behind by the advancing front. Eventually, the dye lifts up, reaches the front (dye is exactly at

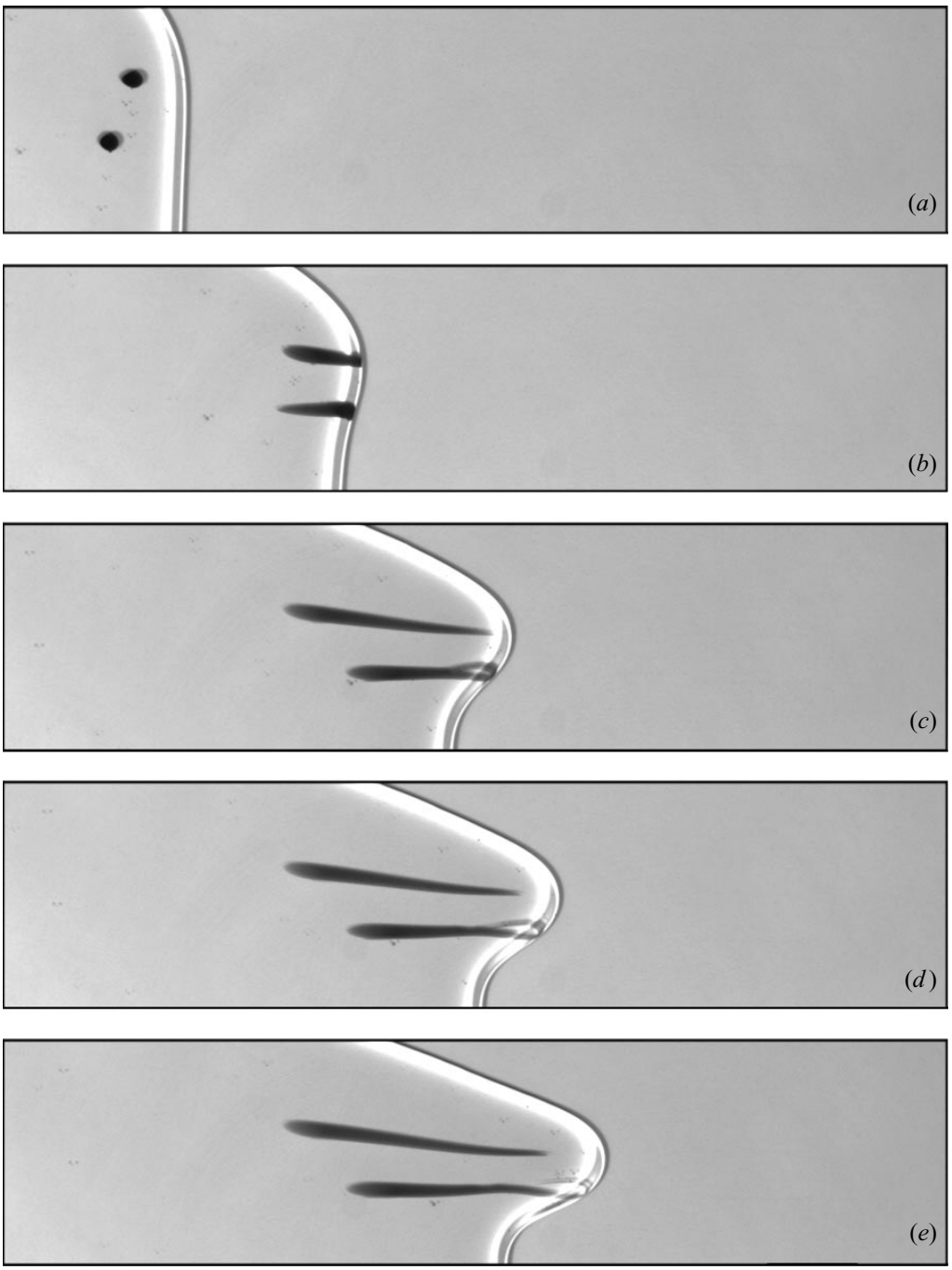

FIGURE 3. Sample top images of dye tracking of the Castor oil front and one of its developing fingers on a dry plane under conditions $(\alpha, \nu, V) = (8^\circ, 9.5\ \mathrm{cm}^2\ \mathrm{s}^{-1}, 150\ \mathrm{ml})$. The frames correspond to the following instants of time (relative to the frame *a*): (*a*) 0 s, (*b*) 9 s, (*c*) 18 s, (*d*) 21 s, (*e*) 24 s. The dye is rolled around the nose forming a 'loop' similar to the glycerine run.

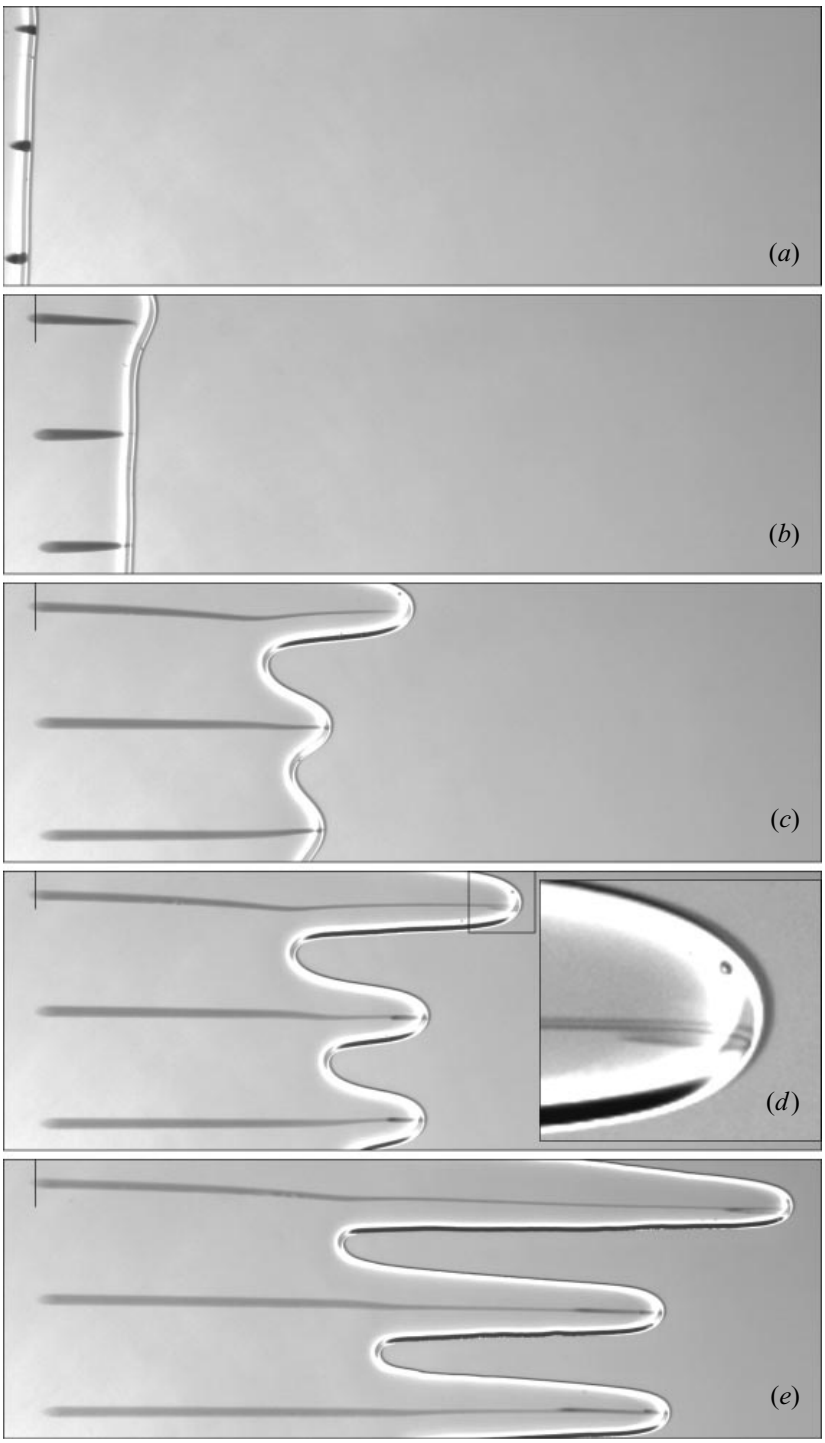

FIGURE 4. Sample top images of dye tracking of the Castor oil front and fingers. All experimental conditions are the same as in figure 3. The frames correspond to the following instants of time (relative to frame *a*): (*a*) 0 s, (*b*) 15 s, (*c*) 37.5 s, (*d*) 52.5 s, (*e*) 100 s. The solid line shows the position of the contact line from frame (*a*) when the 'upper' drop touches the plane. After rotation around the nose, a stretched dye drop from the lower parts of the liquid rises again to the top, reaches the front and continues to rotate around the nose of the finger. The magnification on frame (*d*) shows the second rotation of the dye around the nose of the upper finger. The dye mark on the solid plane, caused by the backward flow under the nose front, is still visible even after 100 s.

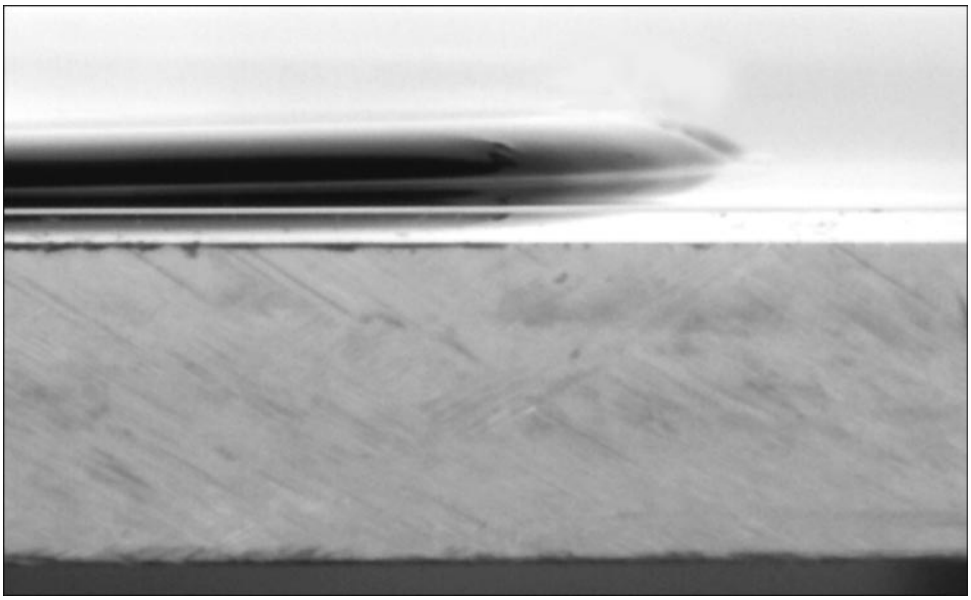

FIGURE 5. Profile image of the gravity-driven Castor oil front on a pre-wetted plane. The experimental conditions (α, ν, V) are (8°, 9.5 cm^2 s^{-1}, 150 ml). The thickness of the Plexiglas plane is 0.8 cm. The plane is covered by a pre-wetted film of Castor oil after draining it for 12 h.

the tips of the two lower fingers in frame *c*) and again rotates around the nose (there are distinct darker dye marks behind fingers on frame *d*). Since coloured Castor oil has a little higher density than the pure liquid, this effect cannot be attributed to the buoyancy of the dye. The magnified image of the Castor oil finger in frame (*d*) shows a similar rotating motion, as for the glycerine front. In figure 4(*e*) one can see the dye marks from two successive rotations of the dye around the nose within the two lower fingers. These successive rotations are slightly different from the first one. The dye thickness now is greater than the original drop and relatively large amounts of dye could keep rotating without touching the plane. At the same time, fingers move slower than the straight front at the beginning. Consequently, the second and following circuits will require less time than the first and the corresponding dye loops will have successively smaller separation. The solid lines in figure 4(*b–e*) show the position of the contact line from frame (*a*), where the upper drop touches the plane. Figure 4(*b*) again indicates the presence of the backward (upstream) flow near the contact line under the moving Castor oil front. Despite the forward stretching of dye by the unidirectional flow in the tail, what remains of the dye spot behind the solid line in figure 4(*e*) is still visible even after 100 s.

3.2. *Flow within wedge fronts on a pre-wetted plane*

Since a straight wedge front of partially wetting fluid is never observed on a dry plane, we have also carried out experiments with Castor oil on a pre-wetted plane to simulate fingering of completely wetting fluids (with $\theta_e \sim 0°$) and to investigate the flow within a wedge front. A typical profile of a spreading Castor oil front before fingering on a pre-wetted plane is shown in figure 5. The front clearly has a wedge shape with $\theta < \pi/2$ and a bump is still absent at the front.

The dye tracking of the Castor oil current on a pre-wetted plane (20 h of drainage) is shown in figure 6. All other experimental conditions are identical to the dry plane

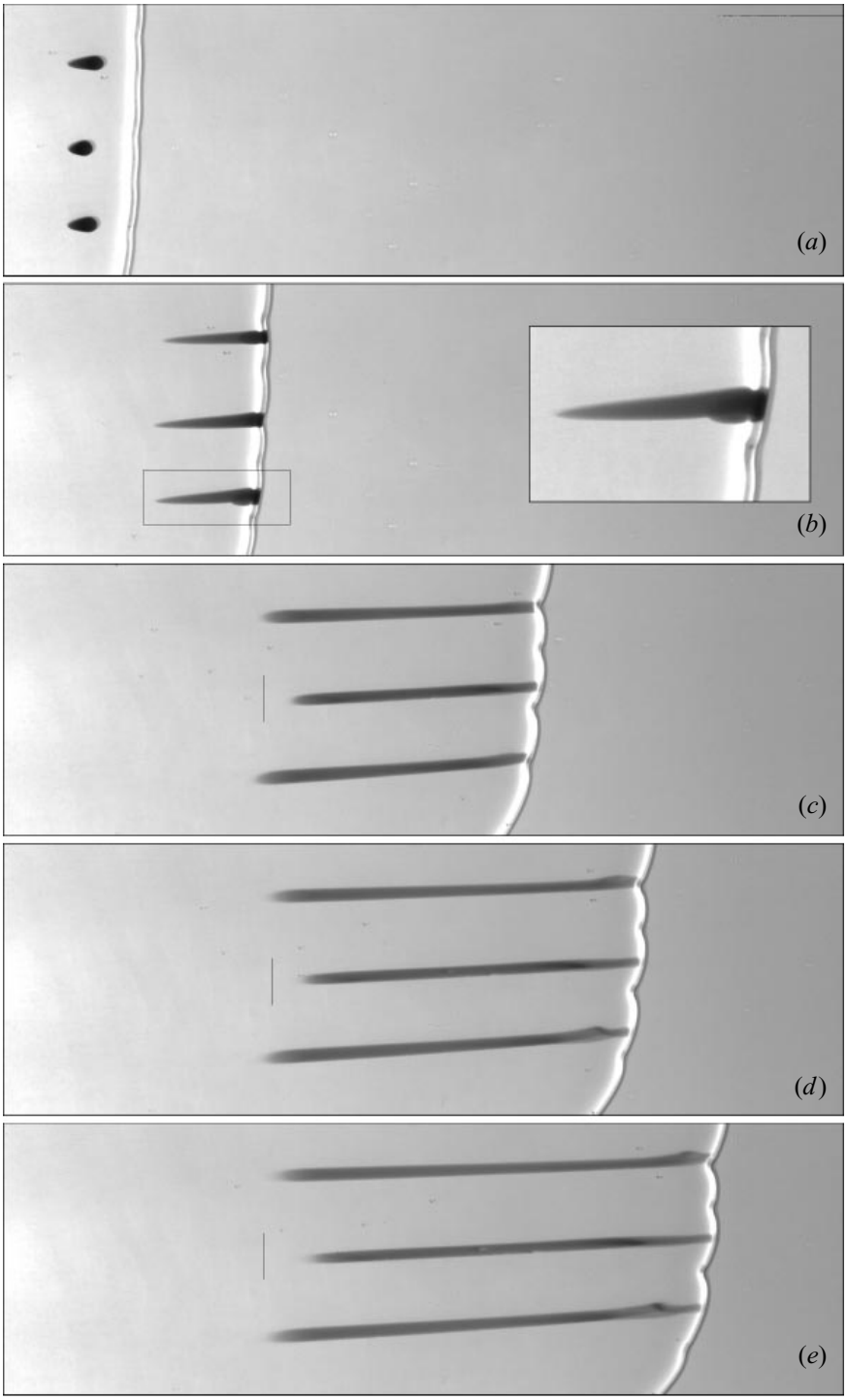

FIGURE 6. Sample top images of dye tracking of the Castor oil front on a pre-wetted plane (20 h of drainage). All others experimental conditions are the same as in figure 3. The frames correspond to the following instants of time (relative to frame *a*): (*a*) 0 s, (*b*) 18 s, (*c*) 78 s, (*d*) 108 s, (*e*) 132 s. The magnification of the lower drop on frame (*b*) shows that a part of the dye (wide) lands on the plane while a thin 'tail' is still on the top interface. The solid line in frames (*c*–*e*) shows the position of the front in frame (*b*) when the central drop touches the plane. Despite a rolling appearance, the flow within the wedge front is unidirectional. Dye does not reach the front again but stays just behind it and does not 'rotate' again in a wedge.

run of figure 4. As one can see from frames (*a*) and (*b*), the motion within the wedge also has a rolling appearance: the drop on the surface is convected to the contact line and lands on the plane. The magnified image of the lowest-drop in figure 6(*b*) shows that the wide part of dye has already landed on the plane when the thin tail is still on the surface. However, there are important differences with the dry plane run that suggest a unidirectional flow field within the wedge. The central drop in figure 6(*b*) just touches the plane and the solid lines on figure 6(*c–e*) show the position of the front at that moment. The relative positions of these lines and the dye marks show that the flow remains unidirectional within the wedge front and liquid near the contact line continues to move forward with the front at a speed slower than the free surface of the current. Stretching or diffusion of the dye cannot be responsible for the observed forward shift of dye marks in figure 6(*c–e*), as one can see from the comparison with dry plane run in figure 4(*b–e*). Another distinction from the dry plane run of figure 4 is that the dye near the plane never lifts up to the top interface. Instead, it stays just behind but never reaches the front (up to the end of our plane) – it does not 'rotate' around the front. The widening dye traces in figures 6(*d*) and 6(*e*) develop behind the front due to secondary transverse currents along the contact line that flow into the growing sawtooth patterns.

3.3. *Fingering from a nose front*

Sample images from the top of the advancing glycerine front and fingers are shown in figure 7. It is evident that the straight front breaks very sharply: the transition from the almost straight front to the pattern with visible tips of growing fingers occurs within the 3 s increment of our frames, which gives about 1–2 cm of distance travelled depending on the inclination angle and viscosity.

After fingering occurs, when θ presumably reaches $\pi/2$, the minima stop almost immediately. For the partially wetting glycerine, the minima are smooth as has been reported earlier (Silvi & Dussan V. 1985; de Bruyn & Jerret 1992). The maxima of the perturbed front accelerate forward relative to the minima and form distinct rivulets (fingers). The speed of the developed fingers is roughly the same as the critical front speed at the onset of fingering while the latter is clearly much slower than that of the thicker film prior to fingering. The width, speed and shape of all primary fingers are almost identical although their separation is very irregular. As the tilt angle α increases, the finger speed and the average finger separation increase while the width decreases. The fingering position $\hat{x}_*$, measured from the back of the plane and the fingers speed are functions of α, liquid volume V and viscosity ν. The width and shape of all primary fingers of the same length are independent of volume and viscosity for a fixed inclination angle ($\alpha = 14^\circ$ in figure 7*d–f*). A total of 15 runs were carried out with glycerine but with different values of α, ν and V.

In some cases (figure 7*b–d*), secondary fingers develop between two primary fingers that are separated further than others. There seems to be a cut-off separation below which no new finger can form. As one can see from figure 7(*b–d*), secondary fingers can only develop from minima with a weak transverse curvature. The secondary fingers are not as wide as the primary ones and do not move as fast.

The fingers retain the nose configuration at their tip with θ close to or slightly larger than $\pi/2$. Dye tracking near a finger in figure 8 shows the same conveyor-belt motion around the nose of the finger as that around the nose of the front in figure 2. The finite width and transverse curvature of a finger drive a secondary flow in the transverse direction that is absent in the straight front. However, this secondary flow

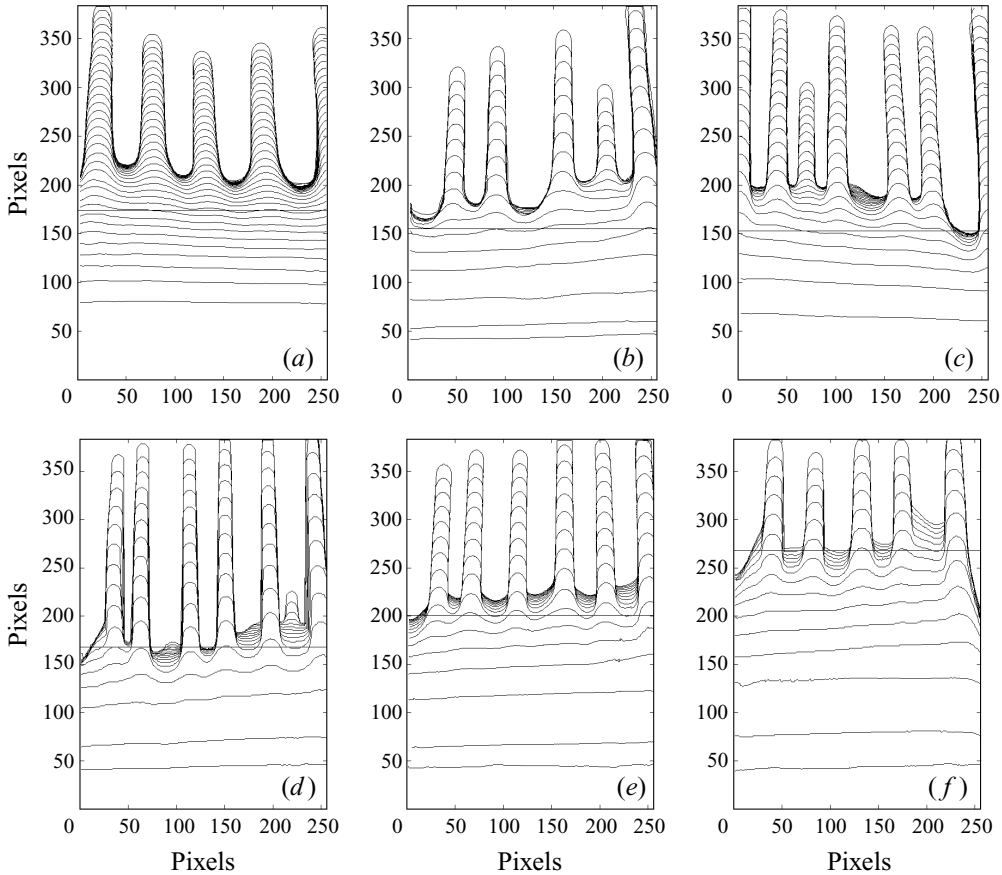

FIGURE 7. Sample top images of fingering for several gravity-driven glycerine fronts under conditions $(\alpha, \nu, V) = (a)\ 6°,\ 7.06\ \mathrm{cm}^2\ \mathrm{s}^{-1},\ 150\ \mathrm{ml}\ (b)\ 8°,\ 4.73\ \mathrm{cm}^2\ \mathrm{s}^{-1},\ 125\ \mathrm{ml}\ (c)\ 10°,\ 6.2\ \mathrm{cm}^2\ \mathrm{s}^{-1},\ 125\ \mathrm{ml}\ (d)\ 14°,\ 6.11\ \mathrm{cm}^2\ \mathrm{s}^{-1},\ 125\ \mathrm{ml}\ (e)\ 14°,\ 6.65\ \mathrm{cm}^2\ \mathrm{s}^{-1},\ 150\ \mathrm{ml}\ (f)\ 14°,\ 8.03\ \mathrm{cm}^2\ \mathrm{s}^{-1},\ 200\ \mathrm{ml}$. The straight horizontal lines are the predicted onset position $\hat{x}_*$ from our theory of (4.15). Secondary fingers (fourth from the left in *b*, third in *c* and sixth in *d*) can form after the primary fingering at $\hat{x}_*$. For the fixed inclination angle, the width and shape of all primary fingers of the same length are almost identical and are independent of ν and V. Images are taken every 3 s. (Each pixel corresponds to (*a*) 1.21 mm, (*b*) 1.18 mm, (*c*) 1.24 mm, (*d–f*) 1.17 mm.

is very weak and the circular dye spot is only slightly dispersed by these currents after it rotates around the nose.

Although θ clearly decreases below $\pi/2$ and approaches the static angle θ_e near the minima after fingering has occurred, the large static contact angle for glycerine ($\theta_e \sim 50° - 70°$) implies that the interval during which θ is between θ_e and $\pi/2$ is very short. Dye drops placed near the minima prior to or after fingering remain stationary or, if they are large enough, spread into the growing fingers. It is hence difficult to decipher the velocity profile within a wedge on a dry plane with $\theta < \pi/2$.

Our experiments on gravity-driven spreading of Castor oil on a dry plane show very similar fingering behaviour as glycerine. The sample top images of fingering for Castor oil fronts on a dry plane are shown in figure 9(*a*). As seen in the figure, the fingers are broader due to the smaller surface tension and the finger separation is more irregular. We should mention that for the almost wetting Castor oil ($\theta_e \simeq 10°$), the minima do not stop completely after fingering but continue to move forward very

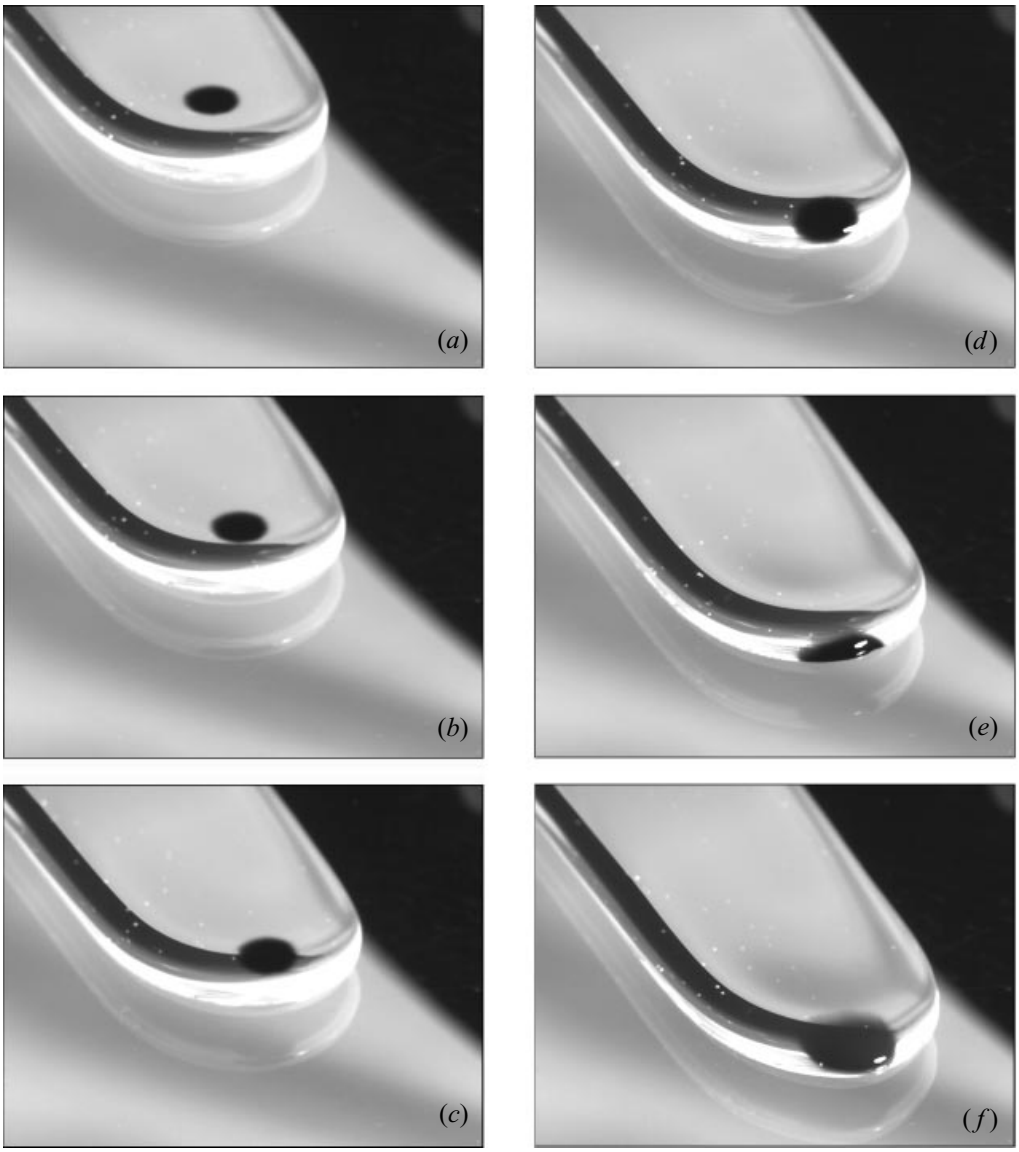

FIGURE 8. Motion of a circular dye drop on top of the interface behind a developed glycerine finger under conditions $(\alpha, \nu, V) = (4^\circ,\ 4.77\ \mathrm{cm}^2\ \mathrm{s}^{-1},\ 150\ \mathrm{ml})$. The dye is again rolled around the nose, indicating a vortex motion, but is dispersed by a secondary transverse flow after it rotates around the nose. Images are taken every 1.5 s.

slowly. Due to this motion and the conservation of total volume, the speed of fingers decreases continuously. Due to the high wettability of Plexiglas by Castor oil, the contact line also moves slowly in the transverse direction. This motion leads to the sharpening of minima between two close fingers and allows the front to adjust its width to create two large side fingers.

The fingering position of both glycerine and Castor oil fronts is insensitive to noise. We find that more careful cleaning of the surface only makes the separation between fingers more regular and has little effect on the fingering position. Large

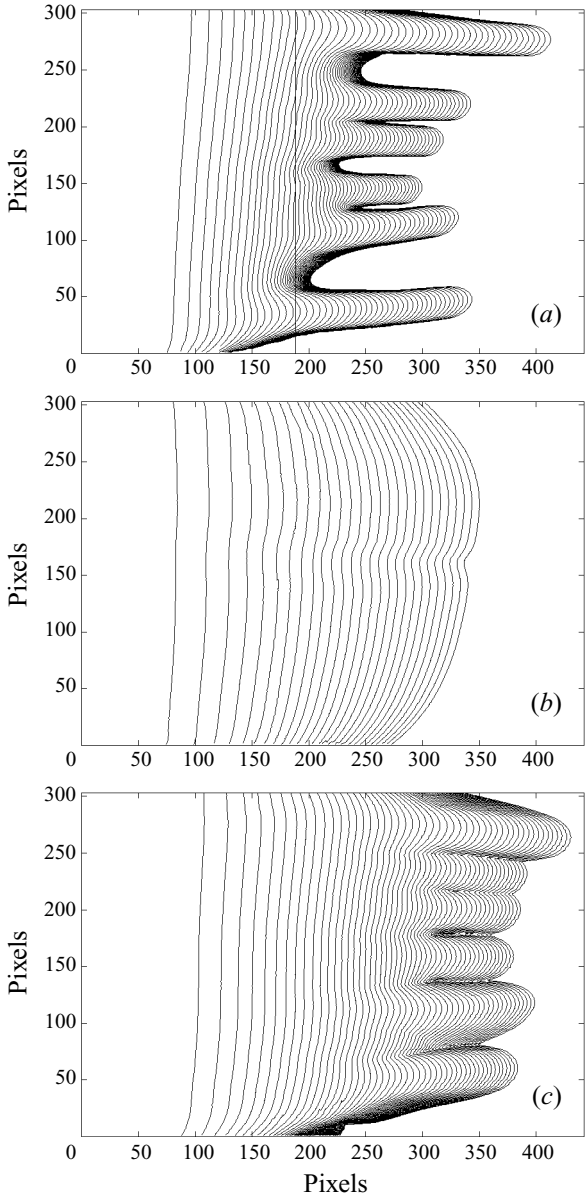

FIGURE 9. Fingering of Castor oil on dry and pre-wetted planes with $(\alpha, \nu, V) = (8^\circ, 9.5\ \mathrm{cm}^2\ \mathrm{s}^{-1}, 125\ \mathrm{ml})$. (*a*) On a dry plane, fingering behaviour of highly wetting Castor oil is qualitatively similar to that of glycerine. The vertical line is the predicted onset position $\hat{x}_*$ from our theory of (4.15). The images are taken every 3 s. (*b*, *c*) The plane is first covered with a prewetting film of Castor oil. Images are taken every 4 s. (*b*) The film is drained for 2 h. (*c*) Drainage takes place for 12 h. The sawtooth patterns, qualitatively similar to that of complete wetting fluid in figure 11, are evident. (Each pixel corresponds to 1.18 mm.)

droplets of liquid or partially pre-wetted surface should be avoided, however, because initially straight fronts accelerate ('jumps') on the wet portions of the plane and a curved front results. However, these large disturbances will not necessary trigger the fingering process if the front thickness is great enough. (Droplets are placed far

upstream from the fingering position $\hat{x}_*$.) Instead, fingers develop further downstream from the curved front. Such a curved front spreads with an oblique angle locally and its fingering position $\hat{x}_*$ is not the same as a straight front. However, the shape of fully developed fingers is almost identical to the shape of fingers developed from a straight front.

To establish that fingering occurs at a critical speed, additional experiments are carried out with glycerine on the second apparatus which drives the contact line at a constant speed. In contrast, the speed slows down monotonically for a gravity-driven front as the film thins and a precise control of the front speed cannot be achieved. In the constant-velocity experiments shown in figure 10, glycerine is driven by gravity initially and is allowed to finger. The driving plate is then turned on and pushes the entire liquid volume from the back at a constant velocity. At the high pushing velocity of figure 10(*a*), the minima are removed and an almost straight front with $\theta > \pi/2$ is restored without any evidence of fingers. In figure 10(*b*), the driving velocity is less than the critical speed for straight contact lines. As such, a steady curved front is established whose maxima and minima move at the driving speed. Fingers do not shoot out relative to the original front or the minima.

3.4. *Fingering from a wedge front*

With the pre-wetted film, the apparent contact angle is always below $\pi/2$ along the contact line before or after fingering. Bumps are also never observed on the front for any thickness of pre-wetted film. To investigate the sensitivity of wedge fronts to surface conditions, we pre-wetted the plane with Castor oil films of different thicknesses. All other experimental conditions, including liquid volume, are carefully chosen to be identical to the dry plane run of figure 9(*a*). As seen in figure 9(*b*), a thick pre-wetted film (only 2 h of drainage) can prevent fingering altogether while fingering still occurs for the thin pre-wetted film of figure 9(*c*) (12 h of drainage). The minima seen in figure 9(*c*) for this case develop the sawtooth patterns of wetting fluid instead of the smooth minima of figure 9(*a*). The fingering position from a wedge is very different from that of a nose as seen in figure 9. It is also very sensitive to the pre-wetted film thickness.

A few sample images of gravity currents of the completely wetting Dow Corning 200 Fluid on a dry Plexiglas plane ($\theta_e \leqslant 1^\circ$, Silvi & Dussan V. 1985) are shown in figure 11. Small drops of coloured Castor oil are placed on the top of interface behind the front. We visually confirm that the front has a wedge shape at the moment when the drops are placed. The developed sawtooth patterns in figure 11(*c*) are qualitatively similar to those of figures 9(*c*) and 6(*c*) formed by the partially wetting Castor oil on a pre-wetted plane. However, all the drops stay on top of the current at all times and have not reached the moving contact line up to the end of the plane. Because Castor oil is immiscible with 200 Fluid and has a lower density ($\rho = 0.961/0.970$ g cm^{-3}for pure Castor oil/200 Fluid) and due to differences in the other physical properties (viscosity, surface tension, etc.), we will not draw any conclusion about the flow within a wedge of complete wetting fluids on a dry plane from these observations. The interfacial flow may not be powerful enough to advect these dyed drops along the wedge down to the contact line.

We also would like to mention that a few tiny air bubbles, which are much smaller than the drops in figure 11, often appear when the liquid is poured into the compartment at the beginning of an experiment. Buoyancy does not suppress the advection of these bubbles under the nose and their circular loops in the moving nose

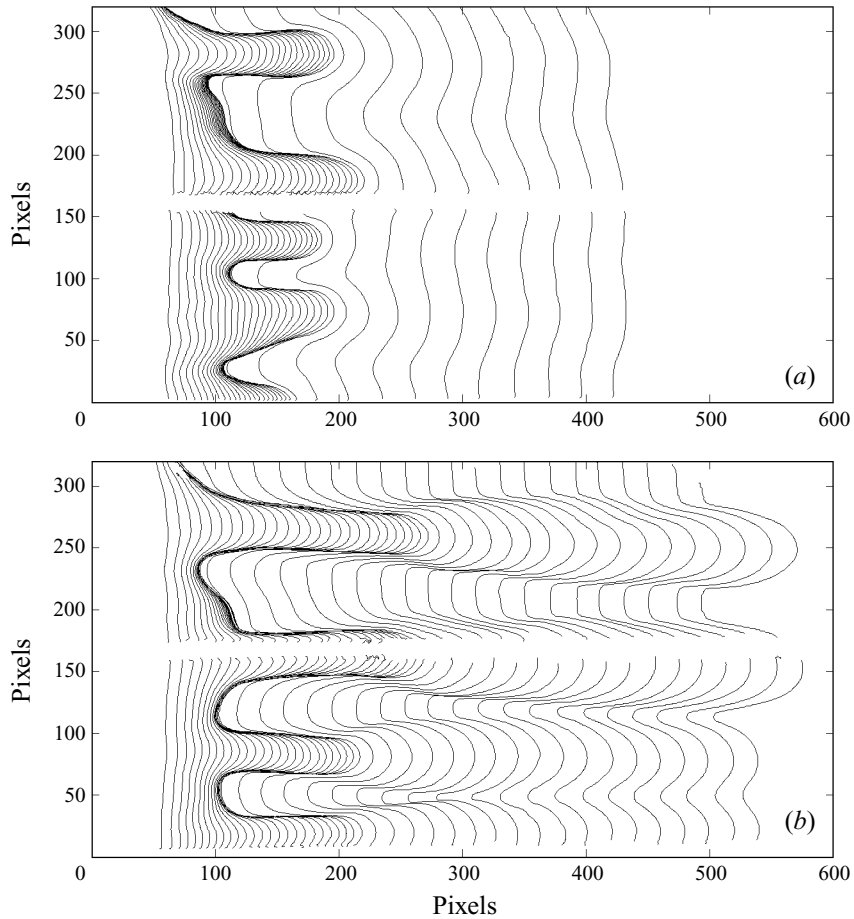

FIGURE 10. Driven contact line for glycerine on a dry plane with $(\alpha, \nu, V) = (5°,\ 3.57\ \text{cm}^2\ \text{s}^{-1},\ 125\ \text{ml})$. Gravity-driven fingering is allowed to take place before the liquid is driven at a constant velocity of (*a*) 1 cm $\text{s}^{-1}$and (*b*) 0.762 cm s^{-1}. The images are taken at 3 second intervals and driving begins at 60 s. The blank region in the middle is obscured by the driving threaded rod. (Each pixel corresponds to 1.47 mm.)

fronts of both glycerine and Castor oil on a dry plane are always clearly visible. In contrast, such rotation of air bubbles is never observed in experiments with the 200 Fluid.

4. Proposed physical mechanism for fingering on a dry plane

4.1. *Motion of nose and wedge fronts*

From the dye tracking experiments (figures 2–4) and from profile imaging of a pre-fingering gravity driven front (figure 1*a*), a straight front of partially wetting fluid moving down a dry inclined plane is characterized by the recirculating vortex within a multi-valued nose. This motion is similar to a deformable wheel, as shown in figure 1(*b*). The contact line itself does not move at all. Instead, a new contact line is created at every instant in time and liquid simply falls down onto the plane. The observed backward (upstream) flow near the solid plane under the moving nose front (figures 2*c* and 4*b*) indicates that the flow remains rotational even in

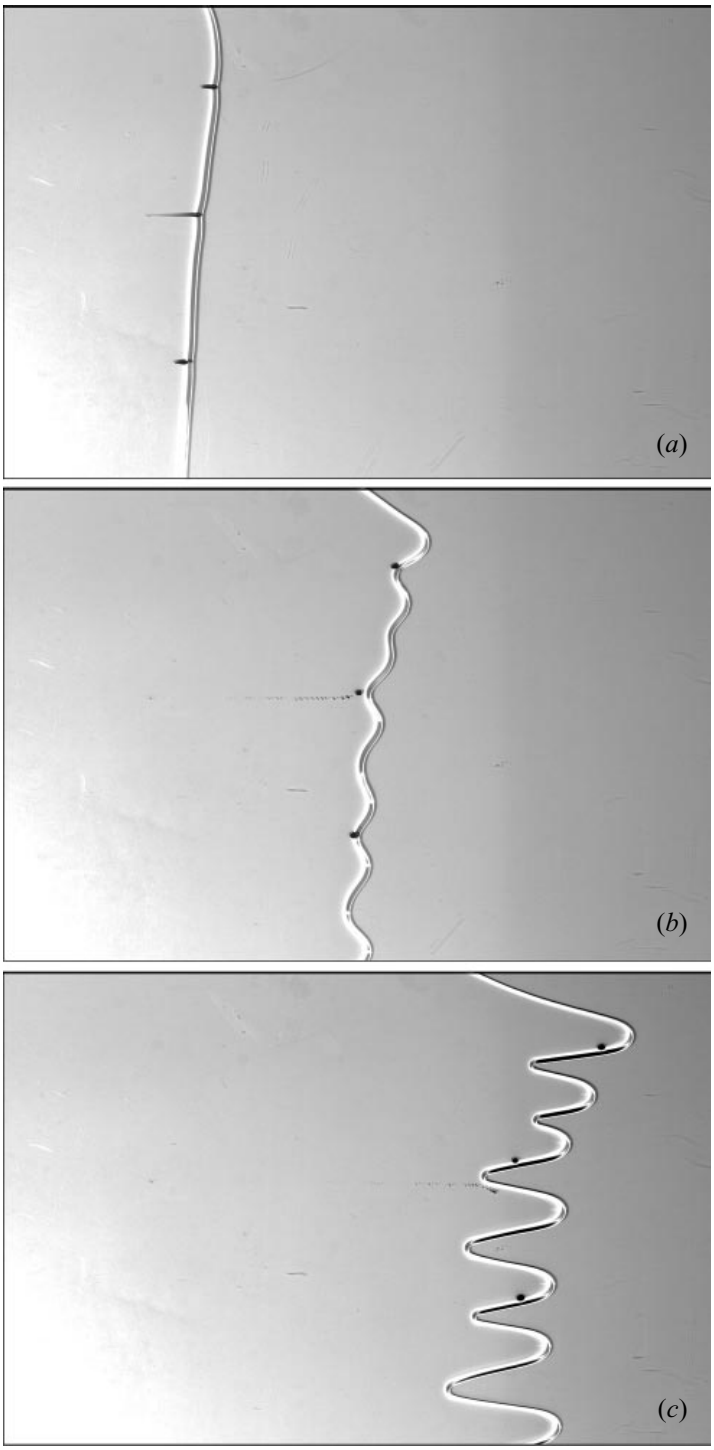

FIGURE 11. Sample top images of fingering of complete wetting Dow Corning 200 fluid on a dry Plexiglas plane. The experimental conditions (α, ν, V) are (8°, 5.00 cm^2 s^{-1}, 150 ml). The frames correspond to the following instants of time (relative to frame *a*): (*a*) 0 s, (*b*) 45 s, (*c*) 111 s. Sawtooth patterns develop. Drops of Castor oil placed on the top interface behind the front, stay on the top and do not reach the contact line. The physical properties (ρ, ν, σ) of pure Castor oil/Dow Corning 200 fluid are (0.961/0.970 g cm^{-3}, 9.5/5.0 cm^2 s^{-1}, 33.1/28.0 mN m^{-1}.)

the laboratory frame. The absence of dye stretching under the moving nose front (figure 2*d–e*) suggests a negligible shear within such vortex motion. The overhanging nose geometry leads to the observed insensitivity of such motion to the surface conditions and wettability of the liquid, as follows from the comparison of data for glycerine ($\theta_e \sim 60°$, figures 1, 2, 7, 8) and for Castor oil on a dry plane ($\theta_e \sim 10°$, figures 3, 4, 9*a*).

It is established in experiments with mechanically driven fronts that there is a critical speed below which a straight nose front cannot exist and that fingering can be suppressed if the front speed is increased beyond a critical value (figure 10).

The shape and speed of the wedge front are sensitive to fluctuations in the contact line region and hence to surface conditions. This is confirmed by the sensitivity of the Castor oil fingering on a pre-wetted plane to the pre-wetted film thickness (figure 9*b, c*).

During the motion of both a nose front on a dry plane and a wedge front on a pre-wetted plane, a liquid particle from the air–liquid interface eventually reaches the contact line and lands on the solid plane, as has been shown by Dussan V. & Davis (1974). However, as is evident from figure 6(*c*), the rotational motion within a wedge is only in a moving frame while the flow field is unidirectional in the laboratory frame. In such a wedge, the fluid motion from the air–liquid to the solid–liquid interface occurs within a microscopic region near the contact line. Independent of the physical mechanism responsible for motion in this region (two-dimensional surface diffusion, evaporation-recondensation, and so on) the speed of the contact line region should be limited. As a consequence, the whole front should move even slower than this limit to sustain the wedge shape of the front. In our experiments with a pre-wetted plane and with completely wetting 200 Fluid, only wedge fronts are detected. It is quite possible that at low inclination angle conditions (a typical value is 8°) the front speed does not exceed the above limiting speed (which should depend on the pre-wetted film thickness) even at the beginning of spreading.

The above observations suggest that recirculating vortex motion within a nose is more preferable energetically than wedge motion. In the case of vortex motion, the velocity decreases from the order of the front speed (on the nose) to zero (on the wall) over the height of the nose that is of the order of the capillary length ($\simeq 2.3$ mm in the case of glycerine). In contrast, the latter length scale for energy dissipation in wedge motion is a molecular length scale ($\sim 10^{-5}$ capillary length).

4.2. *Instability and sensitivity to surface heterogeneity*

Under all conditions at small inclination angles, we do not see a bump on either the nose front or the wedge front (figures 1 and 5). Regardless of the wettability of the liquid, the dryness of the plane or whether the front is mechanically pushed at a constant speed or driven by gravity, a persistent or transient bump is never evident. This is in contradiction to both the instability mechanism and the transient growth mechanism. It is possible that the transient bump cannot be captured experimentally but the nose geometry immediately removes the sensitivity to surface noise required by that scenario.

Fingering of a nose front occurs almost instantaneously at the particular downstream position $\hat{x}_*$, which is insensitive to the surface heterogeneity. This is unlikely for instability or transient growth mechanisms, when fingers should grow from infinitesimal disturbances. The independence of the width and shape of the primary fingers of the same length of the volume and viscosity of liquid for fixed inclination angle (figure 7*d–f*) indicates the hydrostatic nature of the finger tip and hence the unique dependence of the shape on the nose height. The similarity in speed, width

and shape of the primary fingers, the irregularity in their separation and the late appearance of secondary fingers from minima with weak transverse curvature (figure 7) all suggest that fingers of a nose front grow from localized disturbances without much communication between individual fingers. Transverse capillarity simply serves to prevent secondary fingers from developing between two closely placed primary fingers.

These observations suggest that nose fronts are very common for thick films advancing on a dry plane. They are not sensitive to surface noise and do not posses a bump at small inclination angles. As a result, such fronts do not finger by the proposed instability or transient growth mechanisms for wedge fronts. In the next subsection, we offer a physical scenario for the evolution and fingering of gravity-driven currents of partially wetting fluids on a dry plane.

4.3. *Physical mechanism for fingering from a nose front*

At the top of the plane, the straight front moves down by the vortex motion within its multi-valued nose. Such motion is fast due to the large thickness of the front. It is also stable because there is no bump and is insensitive to surface conditions because of the overhanging nose geometry. However, the nose front is only possible if the liquid thickness near the front is sufficiently high. Due to conservation of the total liquid volume, the tail that supplies liquid to the nose thins and decreases the gravity-driven flow rate to the nose. As a result, the nose height decreases as the front spreads forward. The apparent contact angle, which is slaved hydrostatically to the nose height, also decreases accordingly until it reaches $\theta_c = \pi/2$. At this point, the nose geometry and the vortex motion within it cannot be sustained across the entire straight front. The front itself is also very unstable when the apparent contact angle is close to $\pi/2$ because any infinitesimal local disturbances of the front shape along the contact line will change the local mechanism of spreading from vortex motion with low resistance to a unidirectional flow with high resistance and consequently induce a large, finite-amplitude change in the rate of spreading. The front segments with $\theta > \pi/2$ will continue to advance with the original front speed and hence will accelerate relative to segments with $\theta < \pi/2$ which begin to decelerate. At this critical moment, the front hence suffers high-frequency transverse modulations due to the above amplification of small-amplitude noise. In spite of the thinning tail, the fingers can now retain their nose geometry by extracting liquid from the wedge segments that have decelerated. This requires a capillary-driven flow in the transverse direction. As a result, the finger width and separation are determined by capillarity and by how much transverse separation is necessary to ensure sufficient liquid flows into the fingers to sustain their nose geometry. This is consistent with the observed decrease in the average finger separation as the inclination angle of the plane increases. As the primary fingers grow sufficiently in length, they cannot suck liquid from the minima as effectively as at the onset of fingering. Hence, build-up of liquid near the minima with weak transverse curvature becomes possible and secondary fingers can develop.

A switch in the mechanism of motion for a drop on a dry inclined plane across $\theta_c = \pi/2$ has also been proposed by Allen & Benson (1975). It is hence quite reasonable that two spreading mechanisms occur simultaneously along the front of a spreading film at $\theta = \theta_c$ and hence trigger the fingering phenomenon.

4.4. *Derivation of fingering position and speed at $\theta_c = \pi/2$*

Even though it is difficult to measure θ directly, the hydrostatic nature of the nose with a height in excess of the capillary length allows us to theoretically estimate the

fingering position $\hat{x}_*$ and the front speed $\hat{u}_*$ at fingering. This theoretical prediction can then be used to correlate measured fingering data and establish the existence of the noise-independent fingering position at $\theta_c = \pi/2$. For a gravity-driven contact line, this hydrostatic nose must be matched to Huppert's self-similar tail solution

$$\hat{h}_H = \frac{3}{2}\frac{V}{\hat{x}_0}\left(\frac{\hat{x}/\hat{x}_0}{1+\hat{t}/\tau}\right)^{1/2} \tag{4.1}$$

as in earlier analyses for wetting liquids (Troian *et al.* 1989; Bertozzi & Brenner 1997), where $\tau = \left(\nu\hat{x}_0/g\sin\alpha\right)\left(3V/2\hat{x}_0\right)^{-2}$ is the gravity drainage time, V is the cross-section area of the liquid and $\hat{x}_0$ its initial length. The unity constant is often omitted but we choose to retain it here since the onset of fingering often occurs at $(\hat{t}/\tau)$ less than 5.

The inverted parabola in Huppert's solution increases in amplitude downstream until it reaches a sufficiently thick film in the front region. The truncated profile near the front has a high curvature and becomes dominated by capillary effects. However, since our front thickness is in excess of the capillary length, viscous effects are negligible, $O(Ca) \sim 10^{-1}$–10^{-2}, compared to the $O(1)$ gravity and capillary forces. This results in a hydrostatic outer region at the nose. Due to the nose geometry, the full Young–Laplace equation must be used for the hydrostatic outer region instead of the long-wave lubrication approximation. To facilitate matching, we scale Huppert's solution by the capillary length scale $H = (\sigma/\rho g\cos\alpha)^{1/2}$ and the gravitational time scale τ to yield the dimensionless version in a frame of reference x moving with the contact point

$$h_H = \frac{3}{2}\left(\frac{V}{H\hat{x}_0}\right)\left(\frac{x_c+\epsilon x}{1+t}\right)^{1/2}, \tag{4.2}$$

where t and x are dimensionless time and coordinate, $x_c = \hat{x}_c(t)/\hat{x}_0$ is the scaled contact-point position and $\epsilon = H/\hat{x}_0$ is a small number representing the ratio between the capillary length and the initial length of the film. With the same scaling, the Young–Laplace equation in the arclength-angle formulation becomes

$$H_s = \sin\varphi, \qquad x_s = \cos\varphi, \qquad \varphi_s = \delta - h + x\tan\alpha, \tag{4.3}$$

where φ is the angle between the interface tangent and the horizontal, measured in the counterclockwise direction on the air side. As is consistent with (4.2), we choose the origin $x = 0$ to be the contact point. Consequently,

$$\varphi(s=0) = \pi - \theta, \quad x(s=0) = h(s=0) = 0, \tag{4.4}$$

where θ is the apparent contact angle measured from the liquid side. The Lagrangian multiplier δ, corresponding to the capillary pressure at the contact point, needs to be determined from the boundary conditions. The complementary boundary conditions are provided by matching to the Huppert solution (4.2) at a position x_b, where the outer solution has a vanishingly small derivative (and second derivative),

$$\varphi_s = 0, \qquad \varphi = \pi, \quad h = h_H(x_b) = h_b. \tag{4.5}$$

To solve the Young–Laplace equation for the static outer region, we require yet another boundary condition other than (4.4) and (4.5). In earlier studies of the wedge front, the solution was either numerically matched to a flat precursor film (Troian *et al.* 1989; Bertozzi & Brenner 1997) or more analytically matched to a decaying precursor film with the addition of an explicit disjoining pressure term (Kalliadasis & Chang 1994, 1996; Hocking 1993). In both cases, viscous effects are again important

in another inner region at the contact line. While such a region still exists near the contact line for a nose front, the overhanging nose geometry implies that the shape of the hydrostatic nose is independent of the front inner region. This independence of the nose from the contact line region is also consistent with the observed insensitivity to surface conditions. Hence, instead of matching the static nose solution of the Young–Laplace equation to a contact line inner region, we impose a mass conservation condition which then fully specifies the problem. The requirement that the cross-sectional area of the nose A is equal to the cross-sectional area of the part truncated from the Huppert's solution gives

$$A = \frac{1}{\tan\alpha}\left[1 - \cos\theta + \frac{h_b^2}{2} - (\delta + x_b \tan\alpha)h_b\right] = \frac{V}{H^2}\left(1 - \frac{(x_c + \epsilon x_b)^{3/2}}{(1+t)^{1/2}}\right). \tag{4.6}$$

The Young–Laplace equation can then be integrated after imposing (4.4), (4.5) and (4.6) to obtain the capillary pressure δ and the parametric expression for the interface shape in terms of $h(\varphi, \theta)$ and $x(\varphi, \theta)$:

$$\delta = \left(\frac{2}{\cos\alpha}\left[\cos\alpha - \cos(\theta + \alpha)\right]\right)^{1/2}, \tag{4.7}$$

$$h(\varphi, \theta) = \left(\frac{\cos\alpha}{2}\right)^{1/2} \int_{\pi-\theta}^{\varphi} \frac{\sin\zeta \, \mathrm{d}\zeta}{(\cos\alpha + \cos(\zeta - \alpha))^{1/2}}, \tag{4.8a}$$

$$x(\varphi, \theta) = \left(\frac{\cos\alpha}{2}\right)^{1/2} \int_{\pi-\theta}^{\varphi} \frac{\cos\zeta \, \mathrm{d}\zeta}{(\cos\alpha + \cos(\zeta - \alpha))^{1/2}}, \tag{4.8b}$$

where the integrands of the elliptic integrals are singular at $\zeta = \pi$ in the horizontal limit of $\alpha = 0$. The back matching location (h_b, x_b) is given by (4.8) when the upper limits of the integrations are equal to π, $\varphi = \pi$. Note that the front position $x_f(t) = \hat{x}_f(t)/\hat{x}_0$, corresponding to the front end of the nose, protrudes beyond the contact point x_c in (4.2) and is given by $x_f(t) = x_c + \epsilon x(\pi/2, \theta)$. Eliminating x_c and x_b from the matching condition (4.5) and the area constraint (4.6), we obtain a parametric time dependence of the front position $x_f(t)$ through θ (for fixed plane inclination angle α):

$$x_f = \frac{3}{2}\frac{V}{H\hat{x}_0 h_b(\theta)}\left\{1 - \frac{H^2}{V}A(\theta)\right\} - \epsilon x\left(\pi, \frac{\pi}{2}\right), \tag{4.9}$$

$$1 + t = \left[\frac{3}{2}\frac{V}{H\hat{x}_0 h_b(\theta)}\right]^3 \left\{1 - \frac{H^2}{V}A(\theta)\right\}, \tag{4.10}$$

where $A(\theta) = \left(1 - \cos\theta - h_b^2(\theta)/2\right) / \tan\alpha$, $h_b(\theta) = h(\pi, \theta)$ and $h(\pi, \theta)$ and $x(\pi, \theta)$ are given by (4.8). The speed of the front $u = \dot{x}_f$ can be obtained by differentiating (4.9) and (4.10) with respect to θ and combining the results,

$$u = \frac{h_b^2(\theta)}{3\left(3V/2H\hat{x}_0\right)^2}\left[1 - \frac{(2H^2/3V)h_b(\theta)x(\pi, \theta)}{1 - (H^2/V)\left(A(\theta) + \frac{1}{3}h_b(\theta)x(\pi, \theta)\right)}\right]. \tag{4.11}$$

The nose shape prior to fingering at $\theta = \pi/2$ can be described by a single interfacial shape. Since the Young–Laplace equation (4.3) is invariant to a shift in the height $h \to h + h_0$ for a given α, the nose shape is actually universal for all θ as we can see from (4.8). One simply has to shift the solid plane in figure 1(*b*) upwards to obtain

the evolving nose shape prior to fingering for any θ. We have also investigated the sensitivity to the matching condition (4.5) by allowing $\varphi = \varphi_i$ to be different from π at the inflection point $\varphi_s = 0$ where the matching takes place. We are hence allowing for a non-zero slope while insisting on zero curvature at the matching position, curvature being higher order than the slope in the long-wave expansion of the Huppert solution. It is evident in figure 1(*b*) that the nose is not sensitive to changes in the slope of the matching position.

The critical position and the critical time for the beginning of fingering are given by (4.9) and (4.10) with $\theta = \pi/2$. However, these expressions are complicated by the elliptic integral (4.8*a*) for the film height $h_b(\theta) = h(\pi, \theta)$ at the matching location. Fortunately, we can simplify them in the limit of small α at criticality $\theta_c = \pi/2$. We split the interval of integration $(\pi/2, \pi)$ in (4.8*a*) for $h_* = h_b(\pi/2) = h(\pi, \pi/2)$ into two parts from $(\pi/2, \pi-\gamma)$ to $(\pi-\gamma, \pi)$. Due to the definition of $h(\varphi, \theta)$ in (4.8*a*), h_* in terms of these two integrals can be written as $h_* = h(\pi-\gamma, \pi/2) + h(\pi, \gamma)$. A change of variables $\zeta = \pi/2 + \eta$ and $\zeta = \pi - 2\eta$ in the first and second integrals, respectively, yields

$$h_* = \frac{1}{\sqrt{2}} \int_0^{\pi/2-\gamma} \frac{\cos\eta \mathrm{d}\eta}{(1 - \sin\eta + \tan\alpha\cos\eta)^{1/2}} + 2\int_0^{\gamma/2} \left(\frac{\sin\eta}{\sin\eta + \tan\alpha\cos\eta}\right)^{1/2} \cos\eta \mathrm{d}\eta. \tag{4.12}$$

For small α, (4.12) can be approximated as

$$\begin{aligned} h_* &= \frac{1}{\sqrt{2}} \int_0^{\pi/2-\gamma} \frac{\cos\eta \mathrm{d}\eta}{(1 - \sin\eta + \tan\alpha)^{1/2}} + R_1 + 2\int_0^{\gamma/2} \left(\frac{\sin\eta}{\sin\eta + \tan\alpha}\right)^{1/2} \cos\eta \mathrm{d}\eta + R_2 \\ &= I_1 + R_1 + I_2 + R_2, \end{aligned} \tag{4.13}$$

where remainders R_1 and R_2 are both non-negative functions of γ. Differentiating $I_1 + I_2$ with respect to γ with Leibniz's rule shows that the choice $\gamma = \pi/3$ gives a maximum value to the expression $h_* \approx I_1 + I_2$, i.e. it minimizes the remainders $R_1 + R_2$. Integration of (4.13) with $\gamma = \pi/3$ can be easily done and it gives the following closed-form solution:

$$h_* \approx (2(1 + \tan\alpha))^{1/2} - 2\tan\alpha \log\left\{\frac{1 + (1 + 2\tan\alpha)^{1/2}}{(2\tan\alpha)^{1/2}}\right\}. \tag{4.14}$$

Using (4.14) instead of an exact expression (4.8*a*) for $h_* = h(\pi, \pi/2)$ gives an error less than 2% for $\alpha < 20°$. In our experimental range of inclination angles ($4° \leqslant \alpha \leqslant 14°$) the error does not exceed 1%. With the same accuracy, neglecting in (4.9), (4.10) and (4.11) terms of $O(H^2/V)$ and $O(\epsilon)$, which are always smaller than 10^{-1} in our experiments, we obtain the following simplified expressions for the dimensional fingering position $\hat{x}_*$, time $\hat{t}_*$ and speed $\hat{u}_*$:

$$\hat{x}_* = \frac{3}{2}\frac{V}{Hh_*}, \quad \hat{t}_* + \tau = \frac{3V}{2H}\frac{\rho\nu}{\sigma\tan\alpha}\frac{1}{h_*^3}, \quad \hat{u}_* = \frac{\sigma\tan\alpha}{3\rho\nu}h_*^2 \tag{4.15}$$

where $H = (\sigma/\rho g\cos\alpha)^{1/2}$, $\tau = \left(\nu\hat{x}_0/g\sin\alpha\right)\left(3V/2\hat{x}_0\right)^{-2}$ and h_* is given by (4.14).

4.5. *Comparison to fingering data*

In figures 7 and 9(*a*), we favourably compare (4.15) to the actual fingering locations. In figure 12(*a*), the front, one finger and one minimum position $\hat{x}(\hat{t})$ of both the glycerine and Castor oil data on a dry plane from figure 9(*a*) are normalized by $\hat{x}_*$ and plotted against shifted time $\hat{t}+\tau$ normalized by $\hat{t}_*+\tau$ of (4.15). In such a normalization the fingering position, i.e. the beginning of the separation of maxima and minima, must cor-

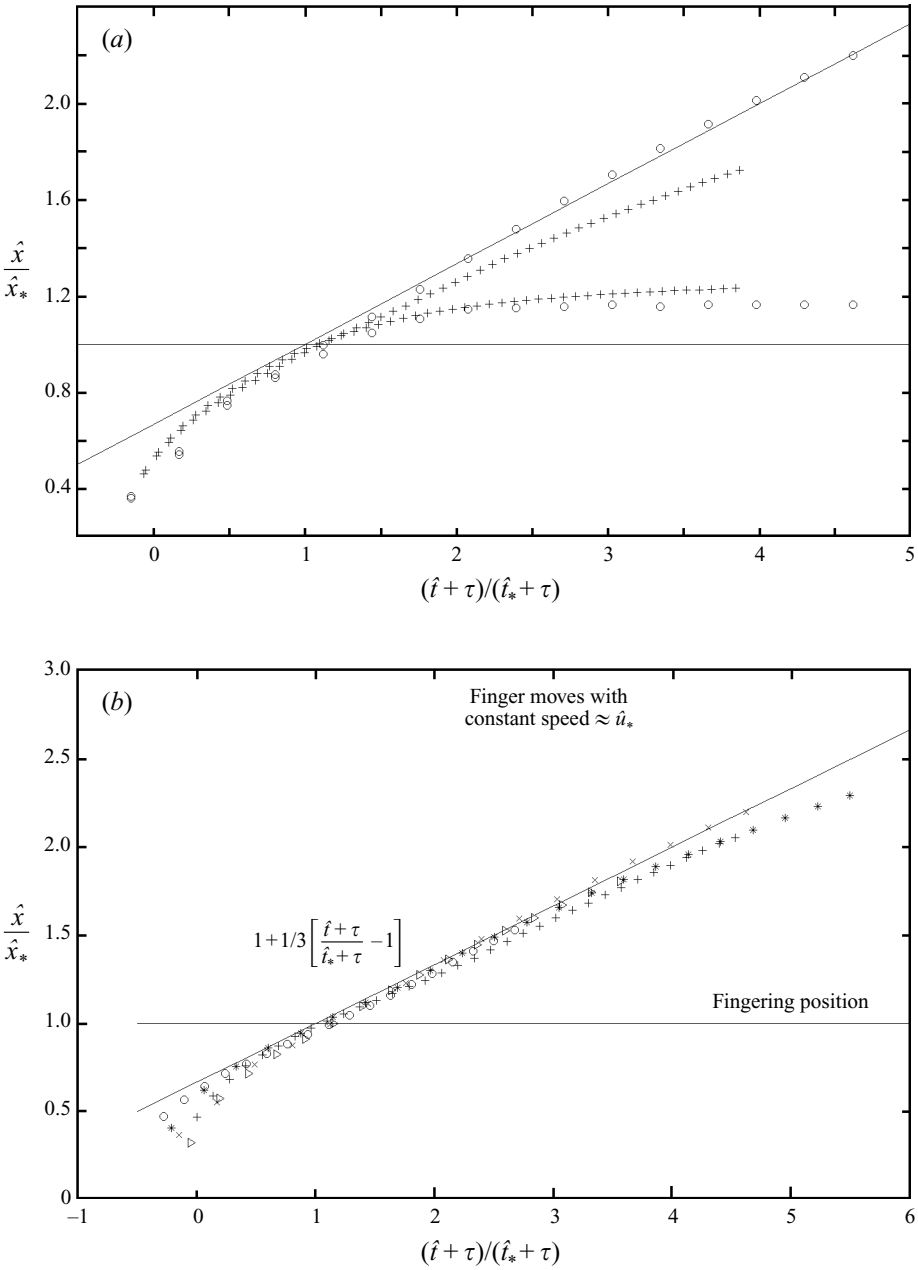

FIGURE 12. (*a*) Normalized position plots for the straight front before fingering and a finger and a minimum after fingering for +, the Castor oil data of figure 9(*a*) over a dry plane with $(\alpha, v, V) = (8°, 9.5\ \text{cm}^2\ \text{s}^{-1}, 125\ \text{ml})$ and ∘, a sample glycerine data of figure 7(*b*) with $(8°, 4.73\ \text{cm}^2\ \text{s}^{-1}, 125\ \text{ml})$. (*b*)Normalized plots of the front and finger position $x_f(t)$ as functions of time for 5 glycerine runs. If fingering is indeed triggered at $\theta = \pi/2$, the normalized curves should pass through the (1,1) grid as they do. Theoretical prediction of the critical speed is also consistent with the data. Conditions (α, v, V) are: ∘, 4°, 3.41 cm^2 s^{-1}, 200 ml; +, 6°, 7.06 cm^2 s^{-1}, 150 ml; ×, 8°, 4.73 cm^2 s^{-1}, 125 ml; ∗, 10°, 6.2 cm^2 s^{-1}, 125 ml; ▷, 14°, 6.65 cm^2 s^{-1}, 150 ml.

respond to the point $(x_*, t_*) = (1, 1)$ and the speed at this point must equal $1/3$. Despite the large difference in viscosity, both normalized curves converge and pass through the (1,1) grid in the normalized plot with almost exactly the predicted speed represented by the slope of the solid line. For glycerine, the minima decelerate rapidly beyond fingering and come to a complete stop, but for Castor oil they continue to move slowly. Hence, while the glycerine fingers continue to move for a long duration with the constant front speed at the onset of fingering, the Castor oil fingers do so for a much shorter period. It should be mentioned that such a long constant speed interval cannot be sustained by a straight front. It is only because liquid is supplied to the fingers from the minima that the fingers can continue to move at the same speed and thickness of the straight front at fingering. Eventually, fingers for both liquids will decelerate.

In figure 12(*b*), the front and one finger position $\hat{x}(\hat{t})$ of 5 glycerine runs are plotted in a normalized plot. As is evident, all normalized data collapse onto a single curve near x_* and t_* with the predicted slope. When other fingers are used, the curves do not deviate appreciably. It is also evident from figure 12(*b*) that the advancing speed of the glycerine fingers is almost identical to the front speed at onset for reasons stated above.

Since the initial spreading immediately after the tilt clearly cannot obey Huppert scaling, we define $\hat{x}_0$ from an image subsequent to the first few. It usually corresponds to the second or third line in figures 7 and 9, representing the position of the front at $\hat{t} = 3$ or 6 s. Consequently, the first few data points in figure 12 can correspond to negative normalized time. As seen in figure 12, the formula (4.15) slightly overestimates the fingering position $\hat{x}_*$ probably because the Huppert shape is never fully realized in our experiments. Another reason for the slight deviation is the uncertainty in time at the beginning of each experiment. (Due to the finite time required for tilting, the front begins to move even before the final inclination angle is reached.) For small inclination angles, this time is negligible in comparison with the fingering time, but for $\alpha = 14^\circ$ these times are comparable.

5. Discussion

Several outstanding issues remain concerning fingering of a forced contact line on a dry plane. We have yet to quantify the large difference between the flow resistances and hence the steady spreading speeds of wedge and nose fronts across $\theta_c = \pi/2$. This requires the inclusion of viscous and molecular forces in the contact-line region for both nose fronts and wedge fronts with θ close to $\pi/2$. We have developed a molecular theory for wedges of partially wetting fluids with arbitrary equilibrium contact angles (Indeikina & Chang 1998). The resulting θ–Ca dependence for Santicizer 405 on silicone treated glass is in quantitative agreement with Hoffman's capillary data. We have also found that, for a glycerine wedge moving on a dry Plexiglas plane, the apparent contact angle approaches $\pi/2$ from below at $Ca \approx 1.5 \times 10^{-2}$. This limiting speed of a steady wedge front depends on liquid wettability but is independent of the outer flow geometry. In contrast, experimentally determined speeds of nose fronts at the onset of fingering, as the contact angle approaches $\pi/2$ from above, are in the range $2.9 \times 10^{-2} < Ca < 8.4 \times 10^{-2}$, depending on the inclination angle of the plane.

The evolution beyond the onset of fingering also is not understood. In particular, the fingers tend to be quite similar and hydrostatic. All primary fingers are almost identical in shape and speed even though they are irregularly spaced. If they are indeed hydrostatic, their width and speed may depend only on $\hat{x}_*$ and can be analysed with the current theory.

There is also the remaining question of exactly when one should expect a nose front instead of a wedge front in a general setting. We have found that a nose always appears when the front is sufficiently thick and the driving force is sufficiently large. If there exists some external body force that pushes liquid forward with higher speed than some largest possible speed of molecular wetting, the front protrudes beyond the contact line and forms a nose. Liquid wettability then becomes inconsequential in such nose fronts sustained by external forces. Such external forces include gravity and the apparent contact angles of noses are hence sensitive to bulk conditions and flow geometry. Consequently, we do not expect a universal correlation between the apparent dynamic contact angle and the front speed, independent of flow geometry, in the case of nose fronts. This is in sharp contrast with the universal $\theta \sim Ca^{1/3}$ dependence for low-θ wedges when molecular forces are important. However, a very high liquid wettability or a thick pre-wetted film on the solid can prevent a nose from forming or reduce the flow resistance jump across $\pi/2$ when the driving force decreases. In any case, we expect contact line resistance to be unimportant for a nose front. There is then no need for an apparent contact angle condition during numerical simulation – one can simply omit the grid point at the contact line as suggested by Goodwin & Homsy (1991).

Fingering from wedge fronts seems to be triggered by a mechanism different from nose fronts. This is already evident from the two widely different fingering positions of figures 9(*a*) and 9(*c*) and sensitivity to the thickness of the pre-wetted film in figures 9(*b*) and 9(*c*). The finger spacing is much more regular for wedges. Instead of a critical condition where two states with two different spreading speeds coexist, as we are suggesting here for fingering on dry planes, it is possible that a noise-sensitive linear or nonlinear instability mechanism is in play for wedge fronts. This mechanism is not fully elucidated although some preliminary concepts have been proposed by Bertozzi & Brenner (1997). The patterns formed after fingering on a pre-wetted plane are quite different from the fingers on a dry plane, as is evident from the Castor oil data of figure 9. It would hence be interesting to decipher the mechanism for pre-wetted planes and to explain and quantify the finger patterns to further verify the difference in the mechanisms for dry and pre-wetted planes (nose and wedge front).

This work is supported by an NSF grant and a NASA grant. We are grateful to M. P. Brenner, J. R. de Bruyn , S. Troian and Y. Ye for stimulating discussions. A. I. was partially supported by the Center for Applied Mathematics and I. V. would like to thank Rich Strebinger for his help in designing the experimental set up.

REFERENCES

Allen, R. F. & Benson, P. R. 1975 Rolling drops on an inclined plane. *J. Colloid Interface Sci.* **50**, 250–253.

Bascom, W. D., Cottington, R. L. & Singleterry, C. R. 1964 Dynamic surface phenomena in the spontaneous spreading of oils on solids. In *Contact Angles, Wettability, and Adhesion* (ed. R. E. Gould), pp. 355–379. Am. Chem. Soc.

Bertozzi, A. L. & Brenner, M. P. 1997 Linear stability and transient growth in driven contact lines. *Phys. Fluids* **9**, 530–539.

Bruyn, J. R. de 1992 Growth of fingers at a driven three-phase contact line. *Phys. Rev.* A **46**, R4500–R4503.

Bruyn, J. R. de & Jerret, J. M. 1992 Fingering instability of a gravitationally driven contact line. *Phys. Fluids* A **4**, 234–242.

Dussan V., E. B. 1976 The moving contact line: the slip boundary condition. *J. Fluid Mech.* **77**, 665–684.

Dussan V., E. B. & Davis S. H. 1974 On the motion of a fluid-fluid interface along a solid surface. *J. Fluid Mech.* **65**, 71–103.

Gennes, P. G. de 1985 Wetting: statics and dynamics. *Rev. Mod. Phys.* **57**, 827–863.

Goodwin III, R. D. 1991 An investigation of a viscous coating flow. PhD thesis, Stanford University.

Goodwin, R. & Homsy, G. M. 1991 Viscous flow down a slope in the vicinity of a contact line. *Phys. Fluids* A **3**, 515–528.

Hansen, R. J. & Toong, T. Y. 1971 Dynamic contact angle and its relationship to forces of hydrodynamic origin. *J. Colloid Interface Sci.* **37**, 196–207.

Hocking, L. M. 1993 The influence of intermolecular forces on thin liquid layers. *Phys. Fluids* A **5**, 793–799.

Hoffman, R. L. 1975 A study of the advancing interface. I. Interface shape in liquid-gas system. *J. Colloid Interface Sci.* **50**, 228–241.

Huh, C. & Scriven, L. E. 1971 Hydrodynamic model of steady movement of a solid liquid/liquid contact line. *J. Colloid Interface Sci.* **35**, 85–101.

Huppert, H. 1982 Flow and instability of a viscous current down a slope. *Nature* **300**, 427–429.

Indeikina, A. & Chang, H.-C. 1998 A molecular theory for dynamic contact angles. To appear in *Proc. IUTAM Symp. on Nonlinear Singularities in Deformation and Flow, Haifa, Israel, April 1997*.

Kalliadasis, S. & Chang, H.-C. 1994 Apparent dynamic contact angle of an advancing gas-liquid meniscus. *Phys. Fluids* **6**, 12–23.

Kalliadasis, S. & Chang, H.-C. 1996 Dynamics of liquid spreadings on solid surfaces. *Ind. Eng. Chem. Res.* **35**, 2860–2874.

Ludviksson, V. & Lightfoot, E. N. 1968 Deformation of advancing menisci. *AIChE J.* **14**, 674–677.

Neogi, P. & Abib, F. 1985 Dynamic contact lines in rotating liquids. *Langmuir* **1**, 747–755.

Silvi, N. & Dussan V., E. B. 1985 On the rewetting of an inclined solid surface by a liquid. *Phys. Fluids* **28**, 5–7.

Spaid, M. A. & Homsy, G. M. 1996 Stability of newtonian and viscoelastic dynamic contact lines. *Phys. Fluids* **8**, 460–478.

Troian, S. M., Herbolzheimer, E., Safran, S. A. & Joanny, J. F. 1989 Fingering instabilities of driven spreading films. *Europhys. Lett.* **10**, 25–30.

Yarnold, G. D. 1938 The motion of a mercury index in a capillary tube. *Proc. R. Soc. Lond.* A **50**, 540–552.